Geomorphic evidence for enhanced Pliocene–Quaternary faulting in the northwestern Basin and Range

Magdalena A. Ellis[1,*], Jason B. Barnes[1,†], and Joseph P. Colgan[2]
[1]DEPARTMENT OF GEOLOGICAL SCIENCES, UNIVERSITY OF NORTH CAROLINA, 104 SOUTH ROAD, CHAPEL HILL, NORTH CAROLINA 27599, USA
[2]U.S. GEOLOGICAL SURVEY, DENVER, COLORADO 80225, USA

ABSTRACT

Mountains in the U.S. Basin and Range Province are similar in form, yet they have different histories of deformation and uplift. Unfortunately, chronicling fault slip with techniques like thermochronology and geodetics can still leave sizable, yet potentially important gaps at Pliocene–Quaternary (~10^5–10^6 yr) time scales. Here, we combine existing geochronology with new geomorphic observations and approaches to investigate the Miocene to Quaternary slip history of active normal faults that are exhuming three footwall ranges in northwestern Nevada: the Pine Forest Range, the Jackson Mountains, and the Santa Rosa Range. We use the National Elevation Dataset (10 m) digital elevation model (DEM) to measure bedrock river profiles and hillslope gradients from these ranges. We observe a prominent suite of channel convexities (knickpoints) that segment the channels into upper reaches with low steepness (mean k_{sn} = ~182; θ_{ref} = 0.51) and lower, fault-proximal reaches with high steepness (mean k_{sn} = ~361), with a concomitant increase in hillslope angles of ~6°–9°. Geologic maps and field-based proxies for rock strength allow us to rule out static causes for the knickpoints and interpret them as transient features triggered by a drop in base level that created ~20% of the existing relief (~220 m of ~1050 m total). We then constrain the timing of base-level change using paleochannel profile reconstructions, catchment-scale volumetric erosion fluxes, and a stream-power–based knickpoint celerity (migration) model. Low-temperature thermochronology data show that faulting began at ca. 11–12 Ma, yet our results estimate knickpoint initiation began in the last 5 Ma and possibly as recently as 0.1 Ma with reasonable migration rates of 0.5–2 mm/yr. We interpret the collective results to be evidence for enhanced Pliocene–Quaternary fault slip that may be related to tectonic reorganization in the American West, although we cannot rule out climate as a contributing mechanism. We propose that similar studies, which remain remarkably rare across the region, be used to further test how robust this Plio–Quaternary landscape signal may be throughout the Great Basin.

LITHOSPHERE; v. 7; no. 1; p. 59–72; GSA Data Repository Item 2015021 | Published online 11 December 2014 doi:10.1130/L401.1

INTRODUCTION

The western North American plate margin exemplifies diffuse deformation across a dynamic tectonic boundary. During the late Cenozoic, this tectonic boundary has evolved from a subduction zone to a transform margin, resulting in right-lateral strike-slip motion along the San Andreas fault system (Atwater, 1970; Stewart and Crowell, 1992), distributed shear in the Walker Lane belt (Henry et al., 2007), and widespread extension across the Basin and Range Province (Atwater, 1970; Faulds et al., 2005; Stewart, 1971; Wernicke, 1992). Stretching from the Sierra Nevada Mountains in the west to the Wasatch Range in the east, the U.S. Basin and Range is characterized by footwall mountain ranges and hanging-wall grabens (basins) that are accommodating roughly east-to-west extension (Fig. 1A; Wernicke, 1992). Although most of the ranges are similar in form (Ellis et al., 1999), they have evolved from normal faults with significant spatiotemporal variations in displacement and slip rate (Wallace, 1987). Despite recent contributions to the nature of active extension in the Basin and Range (Colgan, 2013; Frankel et al., 2011; Gorynski et al., 2013; Lifton et al., 2013), detailed information on the evolution of individual fault systems remains sparse. This may, in part, be because Pliocene–Quaternary changes in fault slip are challenging to identify and often poorly resolved with commonly applied techniques like thermochronology, which have a temporal resolution of 10^6–10^7 yr. Thus, it remains common to rely on fault-plane trenching, seismicity, and geodetics, which have temporal resolutions of 10^0–10^4 yr, to identify active faults, estimate their current motion, and assess their seismic hazard potential (Hemphill-Haley et al., 2000; Personius and Mahan, 2005). Even with all these methods combined, there remains a gap in our ability to resolve fault slip at the critical time scales of ~10^5–10^6 yrs. An emerging approach that may help address this shortcoming is to investigate channel morphologies for clues of past base-level changes caused by tectonic and/or climatic perturbations (Kirby and Whipple, 2012; Whittaker, 2012). We hypothesize that by combining quantitative analysis of landforms modified by evolving tectonics with more established techniques, we may be able to resolve more complete normal-fault slip histories across time scales.

Most of the northern Basin and Range Province underwent a period of rapid extension beginning ca. 17–15 Ma (Fig. 1; Colgan and Henry, 2009; Miller et al., 1999; Snow and Wernicke, 2000; Stockli, 2005; Stockli et al., 2002). The northwestern Nevada Basin and Range is an exception, remaining relatively undeformed until the late Miocene (ca. 12 Ma). This late Miocene and younger extension took place on widely spaced, high-angle normal faults that accommodated less extension than the closely spaced imbricate fault systems and detachment faults found in the Basin and Range to the south and east

*maellis@live.unc.edu
†Present address: Landscape Analytics LLC, Raleigh, North Carolina 27607, USA.

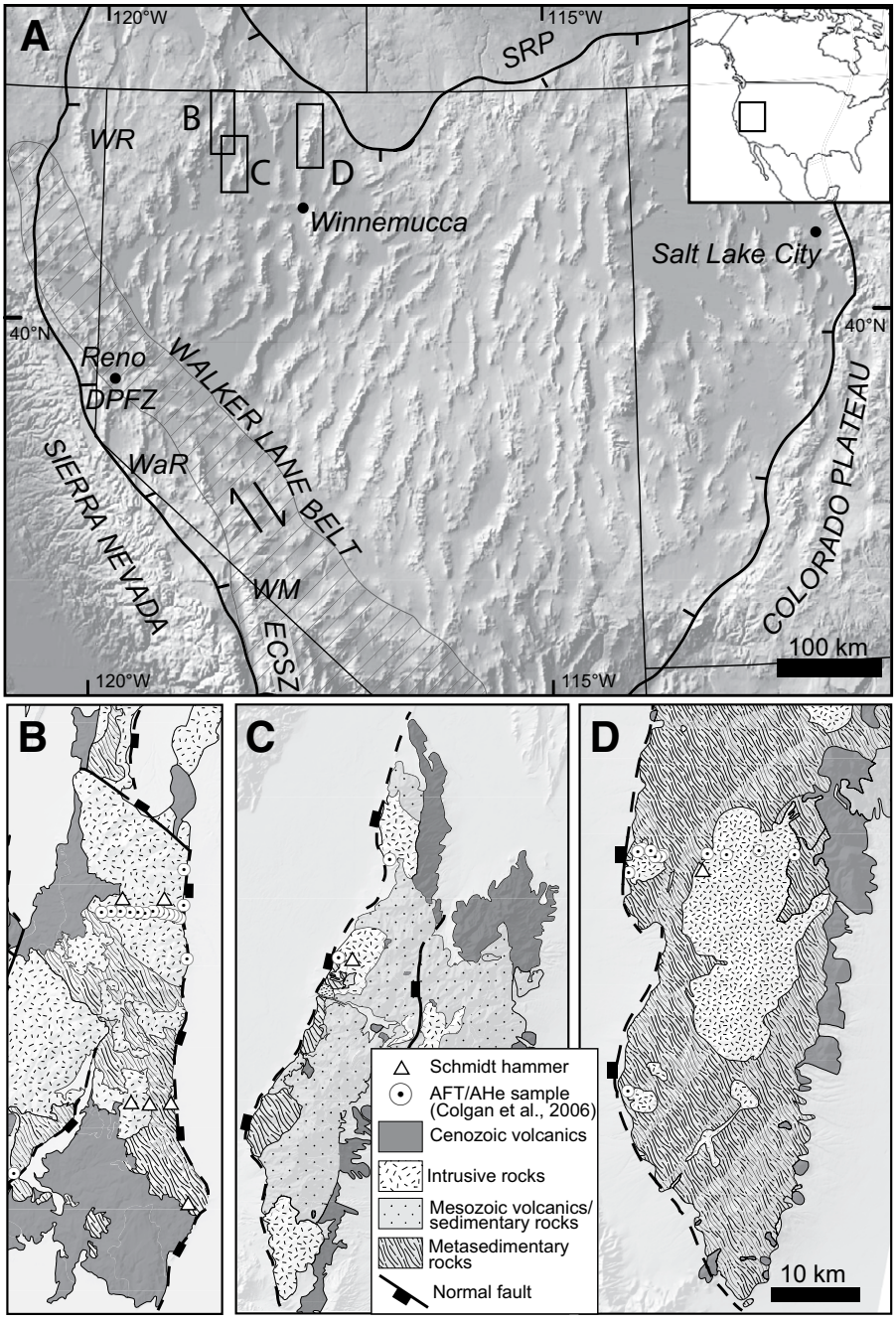

Figure 1. Western U.S. Basin and Range Province with related tectonic provinces, study area ranges, and geographical locations. (A) Topographic relief map of the Basin and Range (barbed black outline). Geologic provinces: Walker Lane belt (striped polygon), Eastern California shear zone (ECSZ), Snake River Plain (SRP), Sierra Nevada Batholith, and the Colorado Plateau. Ranges mentioned in text with Pliocene slip: Warner Range (WR), Wassuk Range (WaR), Donner Pass fault zone (DPFZ), White Mountains (WM). (B–D) Study area geology, thermochronology sample locations (Colgan et al., 2006b), and Schmidt hammer measurement sites in the Pine Forest (B), Jackson Mountains (C), and Santa Rosa (D). Geology is from Faulds et al. (2005); Henry et al. (2007); and Colgan et al. (2006b). AFT—apatite fission track.

(Colgan et al., 2006b). Interestingly, a Pliocene (ca. 3–4 Ma) increase in extension rate has been documented in several places along the western margin of the Basin and Range (Colgan et al., 2008; Henry and Perkins, 2001; Stockli et al., 2003). These observations beg the questions: How widespread is this rejuvenation? Why is it happening? Does it represent slip cessation and renewal or just a change in the rate of ongoing slip?

The purpose of this study is to use footwall catchment morphologies in the U.S. Basin and Range to augment existing constraints on normal-fault slip histories. We present new geomorphic observations from three ranges in northwestern Nevada: the Pine Forest Range, the Jackson Mountains, and the Santa Rosa Range (Fig. 1). Each range was unroofed along a major range-bounding normal-fault system, making them good candidates for investigating the relationships between fault slip and footwall morphology (after Densmore et al., 2004; Harbor, 1997). Thermochronology data show that these tilted, half-graben footwall blocks were exhumed during slip on initially high-angle normal faults beginning in the middle to late Miocene (ca. 12–11 Ma; Colgan et al., 2006b). Our combined field observations, topographic analysis, and knickpoint migration modeling suggest increased fault motion beginning in the Pliocene–Quaternary (ca. 5–0.1 Ma). Our results provide new insights to help characterize Basin and Range faulting histories, with implications for utilizing this approach to improve our understanding of how plate margins accommodate stresses through evolving patterns of deformation.

Background: Tectonic Geomorphology

Active mountain landscapes reflect a dynamic feedback system between tectonic processes that raise Earth's surface and erosion processes that lower it (Montgomery and Brandon, 2002; Schmidt and Montgomery, 1995). Channel incision into rock sets the lower boundary condition for hillslopes, thus dictating the texture and relief structure of the uplifting topography (Whipple and Tucker, 1999). A river in equilibrium with its environment has a smooth, concave-up longitudinal profile where slope decreases systematically with the downstream increase in contributing drainage area (Hack, 1973; Whipple, 2001). Following a change in tectonic or climatic circumstances, streams respond by adjusting their form to reach a new equilibrium condition (Bonnet and Crave, 2003; Tucker and Whipple, 2002). During this transient adjustment phase, rivers possess significant localized convexities, called knickpoints (or knick zones), within their profiles that initiate at local base level and migrate upstream as a kinematic wave (Rosenbloom and Anderson, 1994). As knickpoints move upstream, they separate the lower, transient ("adjusting") portion of the landscape from an upper, relict portion that retains the equilibrium form from the previous conditions (e.g., Clark et al., 2005; Gallen et al., 2013). Geomorphic traits of the relict portion can be used to reconstruct the paleolandscape form because it remains disconnected from the

new conditions until the migrating knickpoint reaches it. Thus, the analysis of channel gradient indices (normalized steepness [k_{sn}], concavity [θ]) and identification of knickpoints are becoming increasingly valuable tools for inferring tectonic patterns and their changes from eroding topographies (Kirby and Whipple, 2012; Whittaker et al., 2008; Wobus et al., 2006a).

Landscapes in steady state possess relationships between their form and the patterns and rates of rock uplift and erosion. For example, fluvial incision models and empirical evidence indicate that uplift rates scale with steady-state channel gradients, such that channels steepen with increased uplift rate (Whipple, 2004). The exact scaling between channel gradient and uplift depends on rock strength, dominant erosion processes, and frequency and magnitude of runoff (Lague et al., 2005). In areas of active extension, increased fault motion results in enhanced footwall rock uplift and contemporaneous lowering of local base level in the adjacent hanging-wall basin. Here, footwall channels strive to maintain equilibrium by steepening, causing an increase in erosion rate. Although channel steepness is not a direct measure of uplift rate, it is useful for identifying patterns of rock uplift (Cyr et al., 2010) despite the fact that the relative impacts of climate and lithology on such a relationship can vary across regions (e.g., Clarke and Burbank, 2011; Stark et al., 2010). In areas where climate and substrate erodibility do not vary much, such as within individual footwall ranges, observed patterns in channel form can be symptomatic of sustained tectonic forcing (Cyr et al., 2010; Harkins et al., 2007; Kirby et al., 2010; Whittaker, 2012).

SETTING

Study Area

We focus on landscapes responding to active extension along three N-S–trending normal fault arrays with primarily dip-slip motion in northwestern Nevada (Fig. 1): the Pine Forest Range, the Santa Rosa Range, and the Jackson Mountains. These ranges lie within ~75 km of each other and are composed of Paleozoic to Mesozoic metasedimentary rocks intruded by Mesozoic plutons. Geologic data show that these pre-Tertiary basement rocks are unconformably overlain by Eocene to Miocene volcanic rocks, which constrain total fault displacement and place upper bounds on the age of fault initiation (Fig. 1A; Colgan et al., 2006b; Noble et al., 1970; Quinn et al., 1997; Wyld, 1996). The Pine Forest Range is bounded by an E-dipping, 50-km-long fault system with a maximum of ~7 km total dip slip, capped by a conformable sequence of 30–16 Ma volcanic rocks tilted up to 30° to the west (Colgan et al., 2006a, 2006b). The Santa Rosa Range is bounded by a 60-km-long, W-dipping fault system with up to ~8 km of total dip slip; overlying volcanic rocks are tilted ~15° east and are 17–15 m.y. old (Fig. 1B; Brueseke et al., 2008; Colgan et al., 2006b). Paleoseismic and luminescence data from the southern Santa Rosa Range yield low slip rates (~0.1 mm/yr averaged over ~400 k.y.) and an elapsed time of 11–16 k.y. since the last earthquake (Personius and Mahan, 2005). The major W-dipping, range-bounding fault system in the Jackson Mountains is 70 km long, with a maximum of ~7 km total dip slip, with overlying volcanics in the northern part of the range that are ca. 15 Ma in age (Fig. 1C; Castor and Henry, 2000; Colgan et al., 2006b; Quinn et al., 1997). The Pine Forest and Santa Rosa range-bounding faults currently dip 35°–40° and are inferred to have originally dipped 50°–55° based on horizontal restoration of the Tertiary unconformities (Colgan et al., 2004, 2006a). The Jackson Mountains range-bounding fault is not exposed, but it is inferred to be ~40°, assuming consistency with the nearby Pine Forest and Santa Rosa Ranges (Colgan et al., 2006b). All three range fronts suggest some degree of past fault segmentation based on the topography of the fault traces, but there is no evidence that the segments are behaving individually any longer (i.e., anomalous topographic highs, structural ramps, or underdisplaced sections), thus we believe them to be past the point of segment interaction.

Apatite Thermochronology

Apatite fission-track (AFT) and (U-Th)/He (AHe) thermochronology can constrain rock cooling histories in the upper ~2–5 km of crust through age determinations from the temperature-dependent retention of radiogenic decay products (Reiners and Ehlers, 2005). AFT ages are completely reset to zero at temperatures >~110–135 °C and are partially reset due to track shortening at temperatures between ~60 °C and 110 °C, called the partial annealing zone (PAZ; e.g., Dumitru, 2000; Green et al., 1989); AHe ages are completely reset to zero at temperatures >~65–80 °C and are partially reset due to partial ^{4}He loss between ~40 °C and 80 °C, termed the partial retention zone (PRZ; e.g., Wolf et al., 1998). The base of the PAZ and PRZ can mark the onset of rapid exhumation, and, along with careful structural control, thermochronologic sample cooling age patterns from an unroofed footwall can be directly related to slip on the bounding fault (Stockli, 2005). We chose the three northwestern Nevada ranges because existing apatite thermochronology data document their exhumation and faulting histories (Figs. 1 and 2; data from Colgan et al., 2006b). Faulting in the Pine Forest Range began 12–11 Ma at a slip rate of 0.3–0.8 km/m.y. (exhumation rate of 0.3–0.5 km/m.y.; Fig. 2). The youngest AHe age is ca. 4 Ma, indicating ~2 km of exhumation (equivalent to cooling from ~65 °C) since that time (Colgan et al., 2006b). Faulting in the Santa Rosa Range also began 12–11 Ma at a slip rate of 0.4–0.8 km/m.y. (exhumation rate of 0.3–0.5 km/m.y.; Fig. 2). The youngest AFT age (AHe dates from the Santa Rosa Range are problematic) is 6.4 Ma, indicating ~3 km of exhumation (equivalent to cooling from ~110 °C) since that time (Colgan et al., 2006b). The initiation and duration of faulting in the Jackson Mountains are less well constrained, but Colgan et al. (2006b) reported AFT and AHe ages of 12 and 7 Ma, respectively (Fig. 2), from one sample near the range-front fault, which they argued

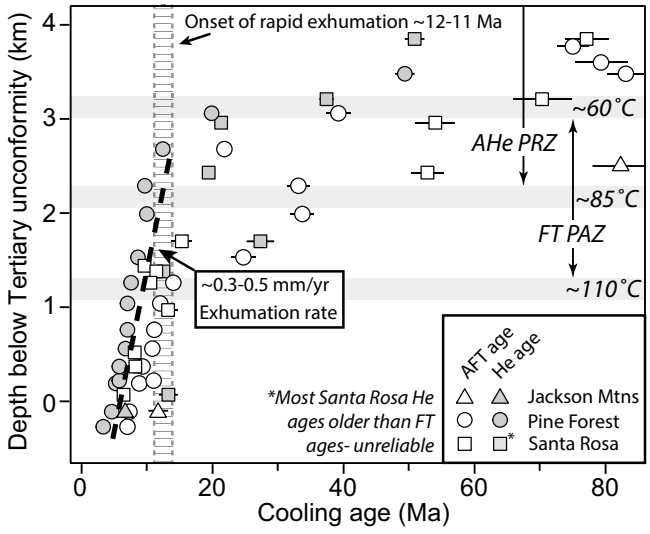

Figure 2. Thermochronology data from the study area ranges (sample locations in Fig. 1). Cooling age (±2σ) versus paleodepth plots for all apatite fission-track (AFT) and (U-Th)/He (AHe) data indicate rapid exhumation began at ca. 12–11 Ma (vertical bar; data from Colgan et al., 2006b). Middle Miocene and younger samples from the Pine Forest Range (circles) and the Santa Rosa Range (squares) show an exhumation rate of ~0.3–0.5 mm/yr. FT PAZ—exhumed apatite fission-track partial annealing zone. AHe PRZ—exhumed AHe partial retention zone.

indicated a similar late Miocene age for faulting as the nearby Pine Forest Range.

Climate

The Great Basin region is generally interpreted to have been a broad highland (the "Nevadaplano") in late Eocene to Oligocene time (ca. 40–30 Ma; Chamberlain et al., 2012; DeCelles, 2004). Prior to the mid-Miocene decrease in mean elevations associated with the development of modern Basin and Range topography, the Sierra Nevada range was already a major orographic barrier (elevation >2 km), blocking air masses and thus precipitation from reaching the Great Basin (Cassel et al., 2012; Horton et al., 2004; Poage and Chamberlain, 2002). This suggests that the first-order climate state was established by the mid-Miocene in our study area. The three ranges have never been glaciated, and the only modern variations in climate are from local, relief-enhanced precipitation that are minor (Ehlers and Gibbard, 2007; Horton et al., 2004). Oxygen isotope and paleobotanical records document a global shift to a cooler climate and enhanced climate variability in the late Cenozoic (ca. 3 Ma; Molnar and England, 1990; Shackleton et al., 1984) that could increase erosion (Zhang et al., 2001) and possibly facilitate channel adjustment in Basin and Range footwalls.

Pliocene–Pleistocene climate cycling caused repeated periods of pluvial lake development throughout the study area. Paleo–Lake Lahontan once occupied every basin in northwestern Nevada; the last and largest highstand occurred ca. 13 ka, when water levels just reached the range fronts in our study area (~1330 m; Morrison, 1991; Reheis, 1999a, 1999b). Since that time the lakes have become progressively smaller, indicative of higher Pleistocene precipitation and a long-term drying trend from the Pleistocene to the present (Reheis, 1999a, 1999b). The pluvial lakes in the Great Basin have always been internally drained, and there is no evidence in the sedimentary record for any removal of mass from the regional basin system (Morrison, 1991). Given this collective information, we choose to assume that tectonics have been, and continue to be, the dominant force affecting local base-level fall and footwall landscape development in the Basin and Range since the mid-Miocene because (1) the relief-enhanced climate gradients are rather minor (~30–40 cm/yr variation across ranges; Daly et al., 2008), and (2) mid-Miocene to recent climate fluctuations are likely subordinate to tectonic-based forcing at the individual range scale (after Densmore et al., 2004; Harbor, 1997; Whipple and Trayler, 1996).

METHODS

Field Data

Lithologic qualities such as composition, fracture density and characteristics, and rock strength exert first-order controls on channel morphology, erodibility, and incision (Allen et al., 2013; Clarke and Burbank, 2011; Montgomery and Gran, 2001; Sklar and Dietrich, 2001). We quantified intact rock strength using a type N Schmidt hammer, a spring-loaded device that measures "rebound" values that scale with laboratory-based measurements of unconfined rock strength (Goudie, 2006; Selby, 1993). We collected rock strength data at eight sites across the ranges: six in Cretaceous granite and two in Paleozoic metasedimentary rocks (triangles, Figs. 1B–1D). We took 40+ measurements at each site and report the mean and standard deviation. We observed fracture presence and characteristics (orientations, degree of mineralization) in the field and concluded that they are uncommon and invariant across the region and hence not likely a controlling factor of erodibility in this region.

Topographic Analysis

Hillslopes

Hillslope gradients can correlate with denudation rates across various mountain settings (Binnie et al., 2007; Harrison, 2000). In active orogens, denudation rates are high but variable because more efficient, erosional processes like mass wasting become dominant above a critical hillslope threshold (~30°; Binnie et al., 2007; Burbank et al., 1996; Montgomery and Brandon, 2002). We calculated hillslope angles using ArcGIS (v. 10) and the 10 m National Elevation Data set (NED) digital elevation model (DEM; Gesch, 2007; Gesch et al., 2002) throughout the main, uplifting footwall catchments; we also measured hillslope angles in the field using a handheld laser range finder at 30 sites from all three ranges (Table DR2[1]) to validate our DEM-based measurements.

Channel Profiles

Topographic relief is set by bedrock rivers that carve valleys between interfluves. The shape of a graded, or equilibrium, river profile is well described by Flint's law, a power-law relationship between local channel slope (S) and upstream drainage area (A):

$$S = k_s A^{-\theta}, \quad (1)$$

where k_s is the steepness index, and θ is the concavity index (Flint, 1974). The concavity index is determined by fitting a power-law relationship to slope-area data from the equilibrium channel reaches, variables easily measured from a DEM (Wobus et al., 2006a). It is common to calculate a regional mean concavity index as a reference (θ_{ref}), which allows for the determination of a normalized steepness index (k_{sn}, in units of $m^{1-2\theta}$/yr), which can then be compared across channel segments with varying drainage area and concavity as follows:

$$k_{sn} = SA^{\theta ref}. \quad (2)$$

Quantifying bedrock river variations with normalized steepness is a common approach for inferring patterns of active tectonics across uplifting landscapes (Cyr et al., 2010; Harkins et al., 2007; Kirby and Whipple, 2012; Wobus et al., 2006b). We analyzed all channels traversing the range front faults that have >1 km^2 drainage area and/or reach the divide (Fig. 3). We used the 10 m NED DEM and codes written in R programming language (version 2.13.1) to conduct the analysis. We smoothed the profile data by resampling the raw elevation data at equal vertical intervals using the contour interval from the original data source (12.192 m [40 ft]; methods after Wobus et al., 2006a). We examined all channel profiles and slope-area data to identify knickpoints, which we define as significant convexities in the profile accompanied by a distinct change in channel gradient ("slope-break" knickpoints; e.g., Fig. 4; Haviv et al., 2010). We calculated θ_{ref} as the mean concavity of the equilibrium (upstream) segments, here $\theta_{ref} = 0.51$. We then calculated (1) k_{sn} along the entire channel reach and (2) a mean k_{sn} for each segment separated by the knickpoint. We next consulted existing geologic maps (Colgan et al., 2006a; Crafford, 2010; Quinn et al., 1997) and the geographic information systems (GIS)–based flow accumulation grid to identify knickpoints coincident with sharp changes in rock type and/or contributing drainage area. We assumed all knickpoints associated with such features to be static effects of them, and all others to be migratory in nature (e.g., Crosby and Whipple, 2006; Miller et al., 2012).

Channel morphology models show that enhanced incision occurs in response to a change in rock uplift rate facilitated by the upstream migration of knickpoints (Kirby and Whipple, 2012; Rosenbloom and Anderson, 1994). Thus, migratory knickpoints are useful for estimating paleotopography because the rel-

[1]GSA Data Repository Item 2015021, extended methodology and raw data, is available at www.geosociety.org/pubs/ft2015.htm, or on request from editing@geosociety.org, Documents Secretary, GSA, P.O. Box 9140, Boulder, CO 80301-9140, USA.

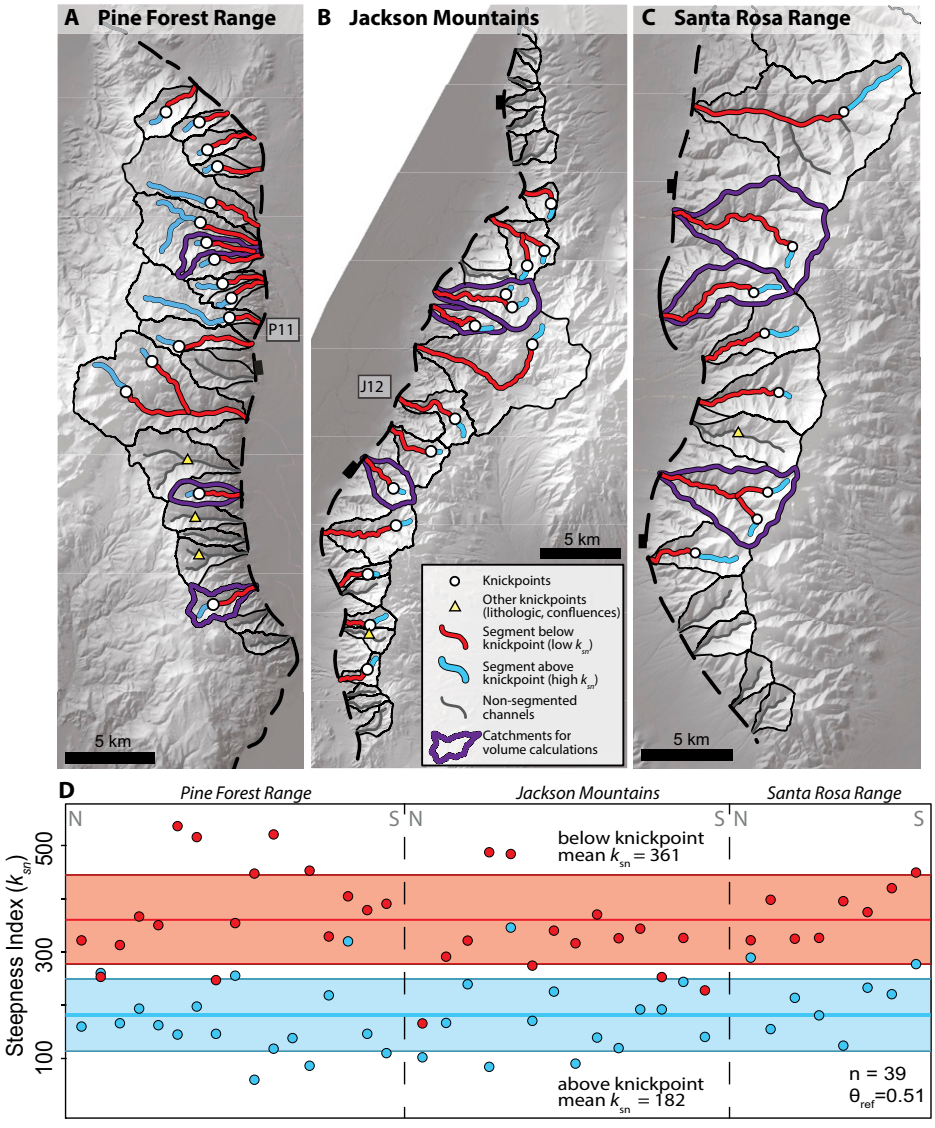

Figure 3. (A–C) Footwall range morphology. Catchments, channel steepness patterns (k_{sn}, θ_{ref} = 0.51), and knickpoints (white circles) of the Pine Forest Range (A), the Jackson Mountains (B), and the Santa Rosa Range (C) (methods after Kirby and Whipple, 2012). Triangles are knickpoints associated with lithologic contacts and/or channel confluences. (D) Mean k_{sn} values for channel segments above (blue) and below (red) the knickpoints. Horizontal color swaths are mean and 1σ for the upper and lower channel reach populations.

ict landscape above them preserves characteristics of the previous equilibrium condition. For every river with a migratory knickpoint, we used the upstream, relict reach of the long profile to extend the paleo-equilibrium channel by extrapolating k_{sn} and θ_{ref} values out to the projected modern fault plane (Fig. 3; after Gallen et al., 2013; Kirby and Whipple, 2012). This allowed us to estimate catchment paleorelief and the relative increase in catchment relief, equivalent to the total amount of channel incision below the relict landscape since the knickpoints formed (Δr in Fig. 4). Note we use "paleorelief" to mean fault-related relief that predated knickpoint formation, not relief that predated faulting. The time between when a knickpoint enters a catchment and travels to its observed position is equivalent to the time required to erode the missing rock volume from the portion of the landscape below the knickpoint (Fig. 5). We estimated knickpoint initiation timing by using a volume-for-time substitution:

$$t_k = (V/A)E^{-1}, \quad (3)$$

where t_k is the time since knickpoint initiation, V is the volume of rock below the knickpoint elevation, A is the drainage area below the knickpoint, and E is the basin-averaged erosion rate (after Gallen et al., 2013; Norton et al., 2008). We computed the maximum possible rock volume eroded by calculating the volume between the modern basin topography and (1) a sloping surface across the modern catchment boundaries, (2) a horizontal surface at the observed knickpoint elevation, and (3) then determining the overlap between the two volumes (Fig. 5B; see Data Repository for details [see footnote 1]).

Existing data sets provide bounds on erosion rates for northwestern Basin and Range topography spanning multiple time scales. Low-temperature thermochronology provides first-order estimates on long-term (m.y.) erosion rates, because AHe ages record the time since a rock cooled through 40–80 °C (Clark et al., 2005; Farley, 2002). In detail, erosion is the surficial removal of mass, and exhumation is rock unroofing (England and Molnar, 1990; Ring et al., 1999). Often considered equivalent, we note that discrepancies between erosion and exhumation rates can arise due to footwall tilting and variations in subsurface heat flow (Ehlers et al., 2001; Ehlers and Farley, 2003). We use a range of 300–500 mm/k.y. for erosion rate (based on the exhumation rates of 0.3–0.5 km/m.y.; Fig. 2), but we consider these values to be near maximum estimates because exhumation rates from one-dimensional age-paleodepth relationships can overestimate surface erosion rates by 10%–40% in normal-fault settings (Ehlers et al., 2001). Cosmogenic ^{10}Be data from footwalls elsewhere in the Basin and Range (Wassuk Range in Nevada, Inyo Range in California, and Stillwater Range in Idaho) with similar climate, lithologies, and morphologies provide shorter-term (10^4 yr) estimates of basin-averaged erosion rates: ~9–100 mm/k.y. for the upper, low-gradient channel reaches and 100–>750 mm/k.y. for the lower, steep reaches (Densmore et al., 2009; Kirby and Whipple, 2012). Conservatively, we used a range of 1–700 mm/k.y. for erosion rate in Equation 3 to calculate the time required to erode the volume of rock from below the knickpoints. We included 700 mm/k.y. as the upper bound to explore this high-rate possibility, but we consider it unlikely because it exceeds the locally measured exhumation rates.

Knickpoint Celerity (Migration) Model

We simulated the velocity, migration, and spatial distribution of knickpoints throughout the ranges using a generic knickpoint celerity model. We did this to test our assumptions that the migratory knickpoints are genetically related and have moved upstream from the range front to their current positions. Another goal in modeling the knickpoints is to corroborate our estimates for

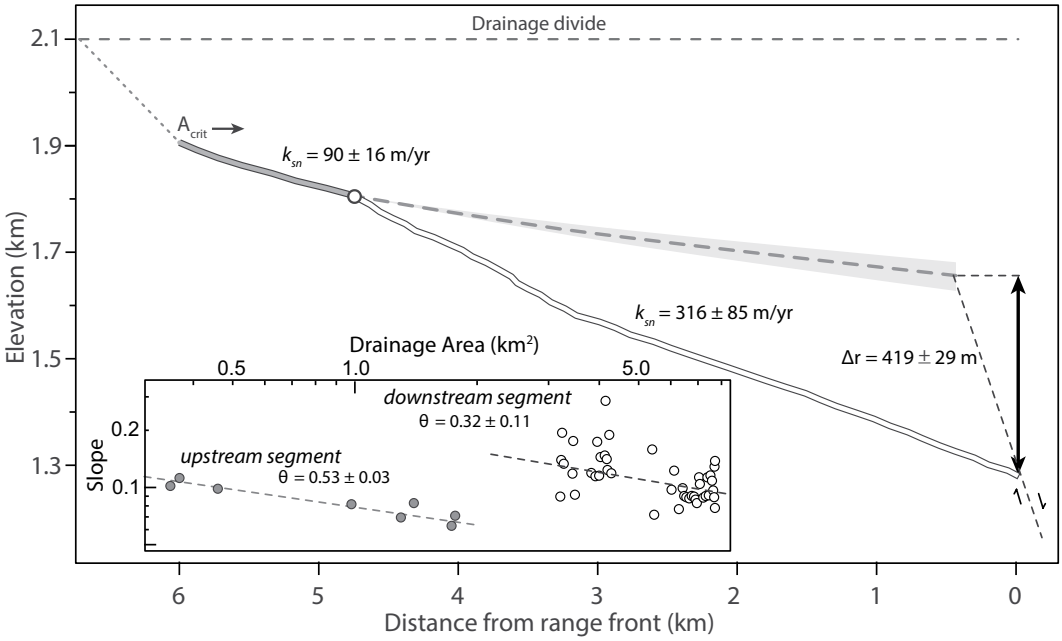

Figure 4. Example channel profile and relict channel reconstruction out to fault plane (location is J12 in Fig. 3B). Reconstruction indicates ~419 m of relief increase since knickpoint initiation. Critical area = A_{crit} = 0.1 km². Fault plane is projected as 50° (vertically exaggerated in figure). Inset is the slope – drainage area data with mean concavities (θ) for the segments above (gray) and below (white) the knickpoint.

the timing of knickpoint initiation and evaluate whether associated migration rates are reasonable compared to existing estimates (Loget and Van Den Driessche, 2009). Knickpoint migration can be described by wave speed, or celerity, and is derived from a detachment-limited stream power incision model that assumes a linear relationship between slope and erosion rate (Rosenbloom and Anderson, 1994; Whipple and Tucker, 1999). Based on this derivation and previous work (Berlin and Anderson, 2007; Crosby and Whipple, 2006; Gallen et al., 2013), the rate of knickpoint propagation can be quantified as a power-law function of drainage area:

$$dx/dt = CA^{p}, \quad (4)$$

where dx/dt is the lateral upstream knickpoint migration rate in m/yr, C is a dimensional coefficient of erodibility in units of $m^{(1-2p)}$/yr, A is upstream drainage area in m^2, and p is a nondimensional constant for power-law dependence on drainage area (Crosby and Whipple, 2006). At each channel pixel in the DEM, we extracted the flow length and upstream drainage area. Using these data, a simulated knickpoint starts at the channel mouth (the range front), traveling upstream and mimicking a pulse of transient incision in response to a change in base level. We employed a brute-force, two-parameter search to find the C and p parameters that minimized the misfit between observed and modeled knickpoint positions within each channel (after Berlin and Anderson, 2007; Crosby and Whipple, 2006; Gallen et al., 2013). For each of seven possible knickpoint initiation times since faulting began ca. 12 Ma (11, 9, 7, 5, 3, 1, 0.5 Ma), we modeled 4800 possible combinations of p and C; we varied p (nondimensional) from 0.3 to 10.5 in 16 increments of 0.05 and C (in $m^{[1-2p]}$/yr) from 10^{-12} to 10^{-4} in 300 logarithmic increments. Knickpoints were modeled as initiating at all three range fronts simultaneously to mimic a regional forcing. We then calculated the misfit between the modeled and observed knickpoints to resolve the best-fitting parameters (detailed in the Data Repository [see footnote 1[; Berlin and Anderson, 2007).

RESULTS

Field Data

Mean rebound values for rocks exposed throughout the three footwalls range from 43.5 to 71.9 (Fig. 6; Table 1). There is high variability

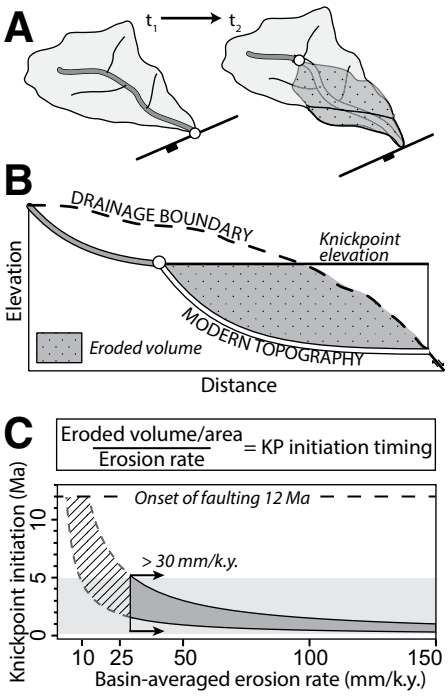

Figure 5. Conceptual model and volume-for-time substitution results for an uplifting footwall range catchment. (A) Schematic catchment evolution from equilibrium (t_1) to transient form (t_2) caused by a base-level fall that triggers knickpoint initiation and migration upstream (after Gallen et al., 2013). Time t_2 highlights the volume of eroded material from below the migrating knickpoint (gray region and white channel). (B) Channel profile-view schematic for estimation of eroded volume at t_2. (C) Knickpoint (KP) initiation timing results based on volume-for-time estimate for catchments in all study area ranges. For erosion rates >30 mm/k.y., the knickpoints initiated <5 Ma. Curves approach zero asymptotically at values greater than 150 mm/k.y. We explored erosion rates up to 700 mm/k.y. (see text for details). Gray bar highlights 5–0.1 Ma, the probable range of knickpoint initiation ages.

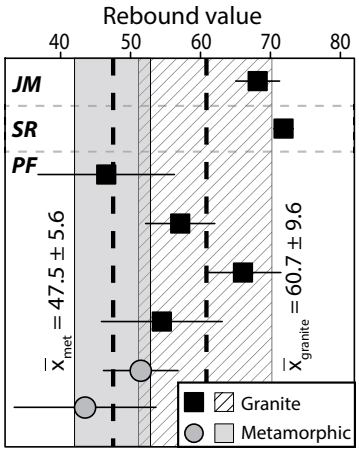

Figure 6. Study area rock strength proxy measurements. Data are mean (±1σ) Schmidt hammer rebound values compiled from various study area locations (see Fig. 1; Table 2). The scatter in mean values and their overlap within error indicate no significant difference in intact strength and hence erodibility between the two main rock types exposed. JM—Jackson Mountains, SR—Santa Rosa Range, PF—Pine Forest Range, met—metamorphic.

TABLE 1. INTACT ROCK STRENGTH FROM SCHMIDT HAMMER

Range	X (UTM)*	Y (UTM)*	Lithology	n	Mean rebound value (± 1σ)
Jackson Mountains	373474	4578799	Granite	40	68.2 ± 3.1
Santa Rosa Range	439609	4602345	Granite	40	71.9 ± 1.4
Pine Forest	364491	4625674	Granite	40	46.5 ± 9.8
Pine Forest	366754	4624723	Granite	40	57.1 ± 4.9
Pine Forest	363575	4609061	Granite	40	66.1 ± 5.4
Pine Forest	365192	4608870	Granite	40	54.5 ± 8.6
Pine Forest	366896	4608744	Metamorphic	50	51.5 ± 5.3
Pine Forest	369368	4600108	Metamorphic	40	43.5 ± 10.1

*UTM zone 11.

in both the granites and the metamorphic rocks: Rebound values on granite range from 46.5 to 71.9, and those for metamorphic rocks range from 43.5 to 51.5. The highest value comes from a stream-abraded, unweathered granite outcrop in the Santa Rosa Range, compared to other localities that possessed some surface weathering and lower rebound values. Although the granitic rocks tend to yield higher rebound values, there is no significant difference in values between the two lithologies within error, defined here and throughout the paper as one standard deviation ($\bar{x}_{granite}$ = 60.7 ± 9.6; $\bar{x}_{metamorphic}$ = 47.5 ± 5.6). Furthermore, knickpoints are rarely observed at lithologic boundaries in the ranges. In conclusion, we see no quantifiable difference in lithology-based rock erodibility.

Topographic Analysis

Hillslopes

Topographic analysis shows that hillslopes are steeper below the knickpoints compared to above them (Fig. 7). In the Pine Forest Range, mean hillslope angles are $\bar{x}_{above}$ = 16° and $\bar{x}_{below}$ = 24°. In the Jackson Mountains, they are $\bar{x}_{above}$ = 23°, $\bar{x}_{below}$ = 30°; in the Santa Rosa Range, they are $\bar{x}_{above}$ = 25°, $\bar{x}_{below}$ = 28°. Field-based measurements spanning all ranges show an identical pattern with a mean value of 20° above and 29° below (Table DR2 [see footnote 1]). These data show that there is consistently a 6°–9° difference between mean hillslopes above versus below the knickpoints. The contrast between slope distributions for hillslopes above versus below the knickpoints suggests a contrast in erosion rates. Erosion rates increase with steeper hillslopes up to a threshold angle of ~30°–35°, at which point erosion rate is controlled by frequency of landsliding (Binnie et al., 2007; Ouimet et al., 2009). Below the knickpoints, which we interpret as transient portions of the channels, the corresponding hillslopes approach threshold angles, whereas hillslopes above the knickpoints do not.

Knickpoints and Steepness Patterns

We analyzed channel profiles from 57 catchments that occupy various along-strike positions within the footwalls adjacent to the three active fault systems (Fig. 3; see Table DR1 for complete results [see footnote 1]). Catchment drainage areas range in size from 0.7 to 59.7 km^2. Catchments from the Santa Rosa Range are substantially larger relative to the others (mean area is 16.8, 6.6, and 8.8 km^2 for the Santa Rosa, Jackson Mountains, and Pine Forest, respectively), which is due to the relative widths of the fault blocks (Densmore et al., 2005). We found 39 knickpoints at similar elevations across 34 different catchments that are not associated with sharp changes in lithology or drainage area (e.g., tributary junctions; circles in Fig. 3; Table 2). Multiple knickpoints within a single catchment signify two main channels, each with a knickpoint at approximately the same elevation. Specifically, we observed 17 knickpoints in 15 (of 22 total) catchments with a mean elevation of 1847 ± 133 m in the Pine Forest Range (Fig. 3A), 14 knickpoints in 12 (of 23 total) catchments with a mean elevation of 1918 ± 103 m in the Jackson Mountains (Fig. 3B), and 8 knickpoints in 7 catchments (of 12 total) with a mean elevation of 2026 ± 148 m in the Santa Rosa Range (Fig. 3C). Catchments that do not possess this primary migratory knickpoint do so

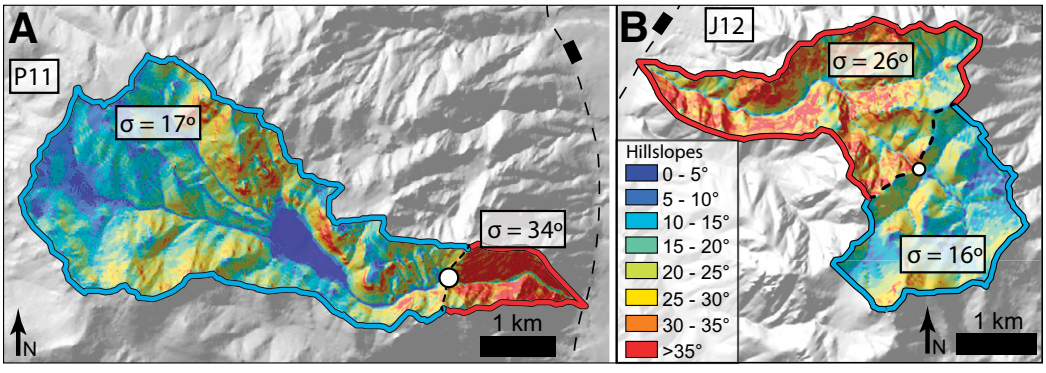

Figure 7. Example catchment-scale hillslope geomorphology (10 m National Elevation Dataset digital elevation model) for (A) Pine Forest catchment P11 and (B) Jackson Mountains catchment J12 (locations in Fig. 1). σ—mean hillslope angle for areas above (blue outline) and below (red outline) the knickpoints. Note that hillslopes are at threshold values (~25+°) below the knickpoints. Dashed line—fault. The low-slope region in the upper P11 catchment is not a standing water body, just very low slopes at a tributary junction.

TABLE 2. DATA FROM CHANNELS WITH KNICKPOINTS

Stream ID	Knickpoint elevation (m)	Distance to knickpoint from range front (m)	k_{sn} above (m/yr)	±1σ	k_{sn} below (m/yr)	±1σ	θ above	±1σ	θ below	±1σ	Mean hillslope above (°)	Mean hillslope below (°)	Change in relief (Δr, m)	Drainage area (km^2)
Pine Forest channels N-S														
P1	1847	2512	160	55	322	80	2.79	0.45	0.37	0.11	26.1	27.6	150	6.20
P2	1959	3658	264	55	257	119	1.15	0.12	0.01	0.12	22.6	28.2	51	4.11
P3	2028	3806	166	33	313	99	1.18	0.07	0.21	0.12	17.7	24.4	54	5.10
P4	1998	2552	197	44	363	136	0.36	–1.11	0.04	0.16	19.4	26.6	124	2.62
P5	1687	3211	163	29	350	84	19.39	1.29	0.09	0.09	17.9	24.1	129	16.31
P6a	1590	1474	145	69	536	220	0.88	–0.05	0.00	0.16	16.8	27.4	125	14.48
P6b	1605	1770	198	49	505	192	0.27	–0.57	0.00	0.16	16.8	27.4	121	14.49
P7	1771	3204	146	92	247	102	0.03	–1.50	0.22	0.17	21.2	25.6	203	3.82
P8	1806	2592	255	66	354	260	0.12	–0.93	0.62	0.25	21.6	23.4	116	3.85
P9	1981	2681	60	43	447	163	1.33	0.12	0.03	0.15	17.4	27.4	512	2.90
P10	1821	1622	118	63	521	198	0.15	–0.81	0.00	0.14	20.2	27.4	404	2.33
P11	1903	2044	126	46	1116	351	0.15	–0.81	0.01	0.13	16.9	33.8	466	12.19
P12	1994	4055	86	32	453	160	0.03	–1.58	3.11	0.11	17.6	27.1	480	8.21
P14a	1859	7212	219	30	329	112	0.11	–0.97	0.47	0.10	23.0	22.0	128	34.39
P14b	1943	8072	320	76	404	131	0.86	–0.06	0.21	0.12	22.1	22.0	96	34.68
P16	1826	2851	146	22	379	128	0.22	–0.65	0.04	0.12	22.4	28.5	253	3.26
P20	1787	2860	110	51	390	110	1.43	0.16	0.09	0.11	18.5	28.3	350	4.69
Jackson Mountain channels N-S														
J6	1740	41836	102	20	166	28	1.12	0.08	0.40	0.07	25.0	30.8	153	3.81
J7a	1928	39125	167	20	291	68	0.34	0.05	0.44	0.08	22.0	28.2	248	9.81
J7b	1990	39125	239	90	321	77	0.55	0.10	0.37	0.09	17.0	27.1	168	9.80
J9a	1892	33229	346	164	484	143	0.56	0.14	0.07	0.09	20.8	29.6	214	10.37
J9b	2143	33229	84	21	487	143	0.68	0.03	0.21	0.11	25.0	29.8	136	10.36
J10	1893	32205	171	32	274	48	0.13	0.07	0.32	0.07	26.9	32.4	189	4.39
J11	1998	29538	226	103	340	92	36.78	0.13	0.39	0.11	33.2	29.0	223	45.06
J12	1801	26094	90	16	316	86	0.53	0.03	0.32	0.11	20.6	33.0	368	7.71
J13	1866	24025	139	46	370	152	0.79	0.07	0.21	0.13	23.9	29.7	368	7.62
J14	1851	21624	120	13	326	63	0.83	0.03	0.29	0.09	25.4	24.2	328	5.91
J15	1919	16262	192	36	344	77	0.43	0.06	0.53	0.08	31.5	29.1	260	12.17
J16	2050	12503	192	29	253	49	0.48	0.05	0.14	0.06	33.9	29.1	148	2.51
J18	1861	10188	244	100	326	113	4.83	0.10	0.02	0.09	26.9	33.8	125	3.25
J20	1925	6503	141	28	228	95	0.41	0.08	0.11	0.13	16.4	32.2	155	3.92
Santa Rosa channels N-S														
S1	1832	9895	289	66	322	137	0.26	0.09	0.10	0.13	22.9	22.6	20	59.71
S2	2095	8171	155	45	398	154	0.49	0.08	0.22	0.16	19.5	25.2	391	27.55
S3	2154	6831	214	104	325	64	0.80	0.14	0.30	0.08	27.4	27.2	221	12.34
S4	1897	4331	181	32	326	63	0.45	0.07	0.24	0.08	27.2	28.0	146	13.01
S5	1945	4979	124	14	395	185	0.25	0.04	1.91	0.12	25.1	28.3	276	17.75
S7a	2258	6694	221	64	420	99	0.72	0.09	0.28	0.10	27.5	29.0	386	18.28
S7b	2103	6513	233	32	375	97	0.39	0.05	0.48	0.09	25.2	29.0	213	18.27
S8	1920	2881	277	50	449	91	0.45	0.06	0.09	0.06	25.6	30.6	132	9.86

for one of the following reasons: (1) The channel head elevation is below the observed knickpoint elevation range of ~1950 m (n = 13); (2) there is a knickpoint at an identifiable heterogeneity such as a lithologic contact (n = 4) or tributary junction (n = 1; triangles in Fig. 3); or (3) there was no identifiable knickpoint observed (n = 6) at our data resolution (gray channels, Fig. 3). Two knickpoints coincident with changes in rock type (of four total) were also within the elevation range of the main observed knickpoint population, and so determining the static versus migratory nature of these knickpoints is ambiguous. The catchments without knickpoints also possess the smallest upstream drainage areas (<6 km^2) and lowest catchment-scale relief (average of ~525 m), and they tend to be near the fault tips (Fig. 3; Table DR1 [see footnote 1]).

The knickpoints divide the channels into two distinct segments (Figs. 3 and 4). The upper reaches above the knickpoints have low steepness (mean k_{sn} = 182 ± 68) compared to the lower reaches, which are characterized by high steepness (mean k_{sn} = 361 ± 84; Fig. 3). Within individual channels, the lower segments are typically 1.5–4 times steeper than the upper segments (e.g., Fig. 4; Table 2). The knickpoints also coincide with steeper hillslopes (mean 24°–30° vs. 16°–25°; see earlier herein). Catchments without migratory knickpoints have intermediate steepness (mean k_{sn} of 247 ± 82), and their hillslopes approach high values (~25°).

Paleoprofile Reconstructions, Base-Level Change, and Incision Volumes

Channel paleoprofile reconstructions show 20–512 m of relief generation since the knickpoints entered the footwall catchments (e.g., Δr in Fig. 4; Table 2). The highest estimates for relief enhancement are from streams draining catchments near the range centers, whereas the lowest estimates tend to be near the tips (Table 2). There is no relationship between the estimated magnitude of increased relief and

drainage area. Despite the wide variability of these relief estimates, the mean value of new relief calculated for each of the three ranges is remarkably similar (221 m, 220 m, and 223 m, in Pine Forest, Jackson Mountains, and Santa Rosa, respectively), suggesting a similar amount of base-level fall across the study area.

The volume of eroded rock from below the knickpoints ranges from 0.06 to 1.2 km^3 (mean = 0.5 km^3). We used a range of erosion rates to back-calculate the timing of knickpoint initiation (Fig. 5): If a catchment eroded more slowly, it would take longer to remove the volume of rock below the knickpoint. If the catchments eroded at an average rate of 30 mm/k.y., a minimum value relative to observed basin-averaged erosion rates in the U.S. Basin and Range, then the knickpoints were generated between 5 and 1 Ma (Fig. 5C). A catchment-averaged erosion rate equivalent to long-term exhumation rates (~300–500 mm/k.y.) requires knickpoint formation ≥0.1 Ma. Therefore, our volume-for-time substitution results require knickpoint initiation between 5 and ≥0.1 Ma.

Knickpoint Migration Model Results

Our knickpoint modeling results show a strong match between predicted and observed knickpoint locations across all 39 knickpoints within the three ranges, which were modeled to initiate simultaneously (e.g., Figs. 8 and 9B). The best-fitting p parameter is consistently 0.45, and the C parameter varies with knickpoint initiation timing, but ranges from 4×10^{-5} to 8×10^{-7} m$^{0.9}$/yr. The lowest misfits between the observed and modeled knickpoint locations are for knickpoints initiating between 5 and 1 Ma (Fig. 9A; Table DR2 [see footnote 1]), but all model runs predicted the observed knickpoint locations with ~1% difference in least sum of squared misfits (LSS). However, because the concomitant best-fit values for C are quite variable, they also result in varying knickpoint migration velocities (see Eq. 3). Knickpoint migration velocities for all knickpoint initiation times explored (11–0.5 Ma) span from ~0.2 to 100 mm/yr. Knickpoints that initiated between 5 and 1 Ma (the lowest LSS result) require migration rates of 0.5–10 mm/yr (Fig. 9A). For example, predicted versus observed knickpoint locations match extremely well (R^2 = 0.85; Fig. 9B) for an initiation age of 3 Ma and a migration rate of 1.5 mm/yr. Assuming all transient knickpoints initiated at the range front simultaneously and traveled upstream as migratory features, our model achieves the lowest misfits for initiation ages between 5 and 1 Ma. However, a wide range of parameters provides good fits, and thus more thorough constraints on erosion rates are required to confirm this time frame for knickpoint initiation.

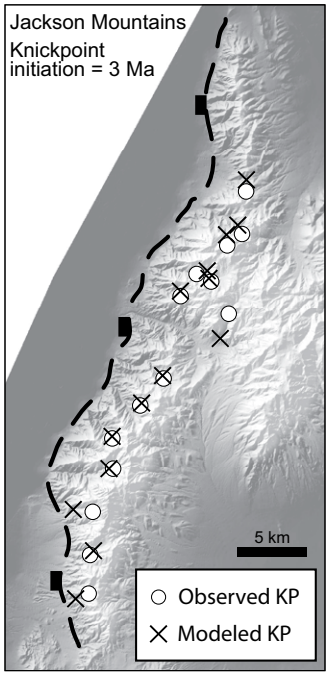

Figure 8. Example map view of modeled vs. observed knickpoint (KP) locations in the Jackson Mountains. Model results with the best-fitting *C* and *p* parameters (1.4 × 10^{-6} m/yr and 0.45, respectively) for knickpoint initiation at 3 Ma. This model requires a knickpoint migration velocity of 1.5 ± 0.5 mm/yr. See Figure DR3 for Pine Forest and Santa Rosa Range results (see text footnote 1).

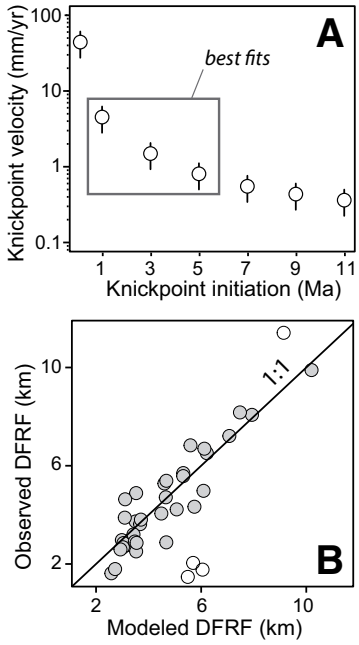

Figure 9. Knickpoint migration model results. (A) Knickpoint migration velocities for best-fit model runs with initiation times of 0.5, 1, 3, 5, 7, 9, and 11 Ma. Results are for all three ranges. Box shows models with best fit (lowest least sum of squares). (B) Predicted vs. observed knickpoint distance from range front (DFRF) for all three ranges from the 3 Ma knickpoint initiation model (migration rate = 1.5 mm/yr). Data fit to 1:1 line have R^2 = 0.85, excluding four knickpoints considered genetically unrelated (white circles; see text for explanation).

DISCUSSION

Channel Patterns Caused by a Change in Fault Slip

There are several possible explanations for our observed channel profile knickpoints and associated steepness patterns. Static knickpoints are associated with distinct, observable geologic phenomena such as faults, landslide deposits, lithologic boundaries, or tributary junctions (Duvall et al., 2004; Korup, 2006; Walsh et al., 2012). This is not the case for the main population of transient knickpoints (n = 39) since we eliminated those possibilities. Furthermore, channels with static knickpoints tend to have peaks in slope on a slope-area plot at the heterogeneity locale rather than a distinct and persistent change in channel slope as we observe (i.e., "vertical-step" vs. "slope-break" knickpoints; see discussion in Kirby and Whipple, 2012). The segmented nature of the channel steepness patterns suggest that they are in a transient state of adjustment to a change in base level. The knickpoints separate upper, relict reaches with low hillslope relief from downstream reaches with 1.5–4× greater steepness and hillslopes that are 6°–9° steeper and near threshold values for the onset of landsliding (e.g., Binnie et al., 2007). Furthermore, the knickpoints are located within relatively narrow altitudinal bands consistent with streams responding to a uniform, sustained forcing such as a change in fault-slip rate. The few channels without knickpoints, in contrast, resemble the downstream, adjusted portions of the streams with migratory knickpoints. When considered in conjunction with their drainage area, relief, and geographic positions, it appears that if a knickpoint had formed in these channels, they have now fully adjusted to the current conditions. These collective observations, combined with our geomorphic analyses and assumptions about the negligible role of climate, lead us to interpret the main suite of knickpoints to be migrating features that initi-

ated ca. 5–0.1 Ma as the result of a sustained change in fault-slip rate.

Modeling and theoretical studies suggest that the vertical rate of knickpoint propagation is a function of rock uplift rates relative to local base level, with higher rates producing higher-elevation knickpoints in a given time (Attal et al., 2008; Niemann et al., 2001; Whittaker, 2012). Faults commonly accumulate displacement by tip propagation and/or segment linkage, resulting in an integrated displacement gradient that increases from zero at the fault tips (i.e., the terminus of the fault) to a central maxima (e.g., Cowie and Roberts, 2001; Dawers et al., 1993). Local constraints on minimum fault throw since fault initiation in our study area (Colgan et al. 2006b; Quinn et al. 1997) suggest that the three fault systems possess long-term deformation rates consistent with this pattern, suggesting they are past the point of segment linkage. However, the knickpoint heights only marginally follow the displacement pattern (Fig. 10). This may indicate that Pliocene–Quaternary deformation rates are distributed more uniformly along strike than the long-term throw data suggest (i.e., they do not display the ideal, bow-shaped distribution). Indeed, if the spatial distribution of displacement rate were more constant along the fault plane, then the knickpoints would fall within similar elevations, as we observe. Our observations of the spatial distribution of knickpoints suggest that the long-term rate of displacement may not follow the same spatial pattern as shorter-term rates. This conclusion is a consequence of normal-fault interaction and growth: Over the lifetime of a fault, long-term patterns of slip do not necessarily mimic short-term patterns as fault segments lengthen, interact, link, and/or cease to grow (Cowie, 1998; Cowie and Roberts, 2001). We present this as a cautionary example of the care that must be taken to account for time averaging when comparing tectonic patterns and geomorphic features.

Changes in climate and basin sedimentation can also cause channels to experience a relative base-level fall. Here, we acknowledge these possible mechanisms for footwall knickpoint formation and rule them out in favor of a change in fault slip as follows. Modern regional base level for all three ranges is the Quinn River, a mud-dominated meandering river located on the floor of paleo–Lake Lahontan (Matsubara and Howard, 2014). This and other paleolakes are symptomatic of excess moisture in the northwestern Basin and Range during the Pleistocene. Increased precipitation would result in an increase in erodibility and thus a decrease in channel gradients (Whipple et al., 1999), which is the opposite of what we observe. In the last ~280 k.y., there have been up to five major highstands in Lake Lahontan, which reached its highest level during the Sehoo highstand ca. 13 ka (Adams and Wesnousky, 1999; Morrison, 1991). If our observed knickpoints formed during the regional fall in base level that followed the last highstand ca. 13 ka, they would have migrated to their current locations at rates ≫100 mm/yr, which is unreasonable (see earlier discussion). Lake Lahontan was big, but in our study area, water levels only reached near the range front during the last highstand (Morrison, 1991; Reheis, 1999a, 1999b), and so we would anticipate minor or negligible aggradation within the mountain interfluves. Given that (1) we observe a steepening of channel gradients, (2) lake levels were relatively low, and (3) the basins were internally drained, we infer that mid-Miocene to recent climate fluctuations are subordinate to tectonic-based forcing in driving footwall landscape development in the study area.

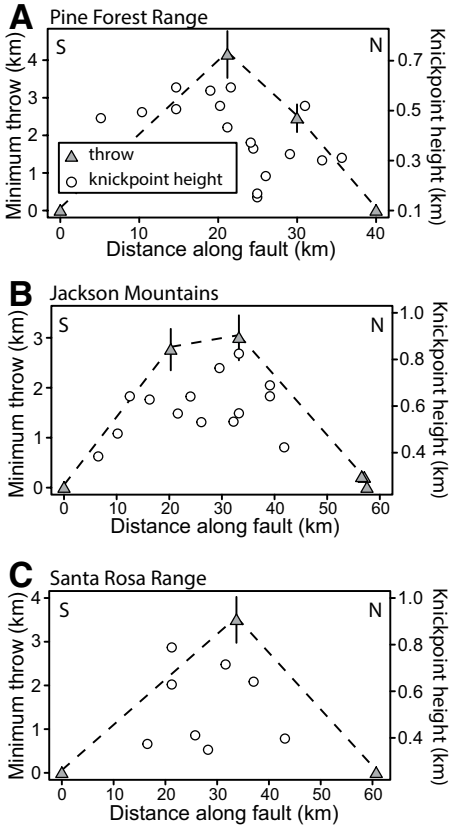

Figure 10. (A–C) Comparison of fault motion and knickpoint position. Minimum fault throw estimates and knickpoint height above the range front are plotted along fault strike for the Pine Forest (A), Jackson Mountains (B), and Santa Rosa Range (C) (from Colgan et al., 2006b; Quinn et al., 1997). In general, maximum knickpoint height and throw fall near the range centers and decrease toward the tips, but this pattern is not robust in places.

Timing and Magnitude of Landscape Adjustment

Rapid exhumation of the footwalls commenced ca. 12–11 Ma, placing an upper limit on any fault-driven changes in topography (Colgan et al., 2006b). Thick sequences of ash-flow tuffs, lava flows, and sedimentary rocks blanketed the study area from the Eocene to the middle Miocene, filling in any previously developed topography on the basement surface and creating a low-relief volcanic plateau prior to the onset of extension (Brueseke et al., 2008; Colgan et al., 2006a; Lerch et al., 2008). This rules out the possibility that the upstream channel segments represent inherited, prefaulting topography (e.g., Densmore et al., 2009). Our channel profile reconstructions estimate an average of 221 ± 126 m (range: 20–512 m) of enhanced, catchment-scale relief across all ranges (Δr in Fig. 4). This means an average of 833 ± 259 m (range: 367–1446 m) of catchment-scale relief predated knickpoint formation. These values are minimums because they do not account for any erosion of the ridge crest or the upper, relict channel reaches. We speculate the large spread in the data represents the nonuniformity of the displacement field and catchment drainage areas along strike, both of which contribute to the variability in Δr; we report the means for purposes of comparison across the study ranges. The lack of regional paleotopography and consistency of paleorelief and Δr estimates across the ranges indicate that, since faulting began, local base level has lowered. Because we propose that enhanced fault slip has facilitated relief creation, we infer that the 20–512 m of new relief is related to the amount of fault throw since slip rate increased.

Our rock volume–for–time substitution analysis provides corroborating evidence for a base-level drop following fault initiation at ca. 12–11 Ma. The exhumation rate of these footwalls from thermochronology is 0.3–0.5 mm/yr (Colgan et al., 2006b). A volume-for-time substitution using an equivalent erosion rate (300–500 mm/k.y.) requires that fault slip increased within the last ~0.5 m.y. Cosmogenic ^{10}Be catchment-averaged denudation rates in the Basin and Range vary from 9 to >750 mm/k.y. (e.g., Densmore et al., 2009; Kirby and Whipple, 2012), with variation within a single range often spanning two orders of magnitude. For example, the Sweetwater Range in southwest Montana has ^{10}Be-derived denudation rates of 9.7–34.8 mm/k.y. at the range front and 9.2–14.2 mm/k.y. in high-elevation

reaches (Densmore et al., 2009). The eastern California Inyo Range has ^{10}Be-derived denudation rates of >750 mm/k.y. at the range front and 40–80 mm/k.y. in high-elevation reaches (Kirby and Whipple, 2012). Given this variability, we explored a range of values (30–700 mm/k.y.) in the volume-for-time substitution analysis, thus bracketing the increase in slip as beginning sometime between 5 and <0.1 Ma (Fig. 5C). This time frame indicates that >200 m of relief was created since 5 Ma and possibly within the last 0.5 m.y., following initial formation of >800 m of earlier fault-related relief. This estimate is consistent with thermochronologic data that show exhumation was ongoing since 12–11 Ma, with the youngest cooling ages indicating 2–3 km of exhumation since ca. 6–4 Ma (Colgan et al., 2006b). With 2–3 km of exhumation (rock uplift relative to the surface) and >200 m (0.2 km) of new relief (i.e., surface uplift) since that time, it requires an erosion rate in the range of 0.3–0.7 km/m.y. (300–700 mm/k.y.). In summary, the data collectively show that enhanced faulting was responsible for increasing footwall relief by 25% of the existing value (~200 m compared to ~800 m pre-knickpoint formation) at the time or ~20% of the total today (>200 m of ~1130 m).

Our knickpoint migration model results support the idea that at least 35 of 39 knickpoints initiated at the same time and migrated upstream across the ranges. Based on large spatial misfits (>2 km), four observed knickpoints may not be related to the main population (white circles in Fig. 9B). One Jackson Mountain knickpoint location is underpredicted by ~2 km. The knickpoint is in a catchment coming off a large paleovalley in the middle of the Jackson Mountains (Fig. 3B). This knickpoint may have originated at the catchment mouth within the paleovalley rather than where the paleovalley reaches the range front ~5 km away, or it may represent an underdisplaced portion of the fault still undergoing segment linkage. Three knickpoint locations (two of which are tributaries in the same catchment) in the Pine Forest Range are overpredicted by several kilometers (white circles in Fig. 9B). It could be that these knickpoints are: (1) associated with a more recent event and hence have not propagated as far upstream or (2) "stuck" on an undocumented mechanical boundary. Another possibility is that the model makes the necessary assumption that drainage area is constant through time, i.e., that the catchments do not lose area to neighboring catchments (lateral divide migration) nor does the main range boundary move (Goren et al., 2014; Willett et al., 2014). Drainage divide migration would affect the model goodness of fit. That said, some degree of misfit is expected when fitting a model to such a large population (e.g., Gallen et al., 2013), but the cumulative misfit between observed and modeled knickpoint locations is so small that the results support the notion that they are genetically related to a change in fault-slip rate.

The best results from our knickpoint migration modeling signify that they formed at the range fronts within the last 5 m.y. and migrated upstream at a rate of 0.5–10 mm/yr (Fig. 9A). Other areas that have similar drainage areas and lithologies, as well as C coefficients that fall within our assumed range, have comparable migration rates of <1–10 mm/yr (Bishop et al., 2005; Hayakawa and Matsukura, 2003; Loget and Van Den Driessche, 2009). In our model, the erosional coefficient, C, varies by over an order of magnitude to adjust to the prescribed knickpoint initiation times, but the high values of C that correspond to the youngest initiation times (younger than 0.5 Ma) require knickpoint velocities that are beyond reasonable values given the setting. Knickpoint migration velocities high enough for the convexities to have initiated within the last 0.5 Ma are ≥100 mm/yr; migration rates of this magnitude are only observed in areas with primarily alluvial substrate or large drainage areas (>100 km^2), neither of which applies here (Loget and Van Den Driessche, 2009). Erosion rates low enough for the knickpoints to have initiated prior to 5 Ma are ≤30 mm/k.y.; erosion rates of this magnitude are not supported by the thermochronology data and are only observed in upper, relict portions of catchments with lower overall relief than those studied here (e.g., the Sweetwater Range in Idaho; Densmore et al., 2009). However, without local constraints on the C coefficient, we cannot rule out the possibility that it could fall outside the range of model best fits and hence vary the knickpoint initiation timing further. That said, because knickpoint migration rates are unlikely to be >100 mm/yr here, and sustained erosion rates are unlikely to be <30 mm/k.y., we favor the interpretation that these knickpoints initiated between 5 and 0.1 Ma (gray bar, Fig. 5C).

What Caused an Increase in Fault-Slip Rate?

Multiple deformation phases have been recognized in the western Basin and Range since late Oligocene time. For example, the Warner Range, ~150 km west of our study area in northeast California, has a two-phase extensional history with the most recent phase of increased slip commencing ca. 3 Ma (Fig. 1; Colgan et al., 2008). Similar renewed Pliocene (ca. 4–3 Ma) extension has been documented in the White Mountains (Stockli et al., 2003) and Inyo Mountains (Goren et al., 2014) in eastern California, the Wassuk Range in western Nevada (Gorynski et al., 2013; Stockli et al., 2002), and in the Donner Pass fault zone near Reno, Nevada (Henry and Perkins, 2001) (Fig. 1). It has been hypothesized that the Walker Lane belt in western Nevada, a region of left-stepping, en-echelon faults with a dextral slip component and high seismicity, began propagating northwestward ca. 9–3 Ma, causing strike-slip deformation in northwestern Nevada (Fig. 1; Faulds et al., 2005). This propagation was approximately coeval with vertical-axis rotations in northwestern Nevada (Cashman and Fontaine, 2000), and a change in motion of the Pacific plate relative to North American plate motion at ca. 8 Ma (Atwater and Stock, 1998). Furthermore, there is evidence for uplift and incision of the Sierra Nevada between 3 and 1.5 Ma (Stock et al., 2005) and <5 Ma (Wakabayashi and Sawyer, 2001). Although the precise nature and timing of this observed enhancement of deformation differ in places, most concur that it is a reflection of the diffuse deformation associated with the Pliocene–Quaternary evolution of the western North American plate margin (Cashman and Fontaine, 2000; Faulds et al., 2005; Henry and Perkins, 2001). Our observations contribute to this growing body of evidence for the Pliocene–Quaternary rejuvenation of deformation within the western Basin and Range.

Increased slip rate can also be attributed to the evolving geometry of a fault system independent of a change in external tectonic forcing. Large, crustal-scale fault systems tend to grow by the amalgamation of multiple segments. As the segments interact and become mechanically linked, they come to behave as one fault equal to the combined length of the two segments with displacement reaching a maximum at the collective fault center (Cartwright et al., 1995; Cowie, 1998; Dawers and Anders, 1995; Gupta and Scholz, 2000). Segment boundaries are often initially locations of anomalously low displacement (Gupta and Scholz, 2000; McLeod et al., 2000), but they ultimately experience slip-rate enhancement due to evolving Coulomb stress changes in the upper crust (Cowie, 1998; Cowie and Roberts, 2001). These faults appear to be matured past the point of segmentation, with the possible exception of the northern Jackson Mountains. Thoroughly determining the timing of formation, propagation, and interaction of each fault segment within our study area is beyond the scope of this study, but we recognize that segment linkage and associated slip enhancement in this region could be the cause for some localized knickpoint anomalies.

Evolving plate-margin kinematics facilitating a change in regional deformation style

in the western Basin and Range are consistent with our principal interpretation: that transient channels are adjusting to a change in fault-slip rate throughout fault-array systems within an ~100 km^2 area in northwestern Nevada since ca. 5–0.1 Ma. Further investigations into footwall morphologies throughout the Basin and Range may help test (1) the robustness and/or widespread nature of this Pliocene–Quaternary landscape response, especially farther east into the more central Basin and Range, as well as (2) whether there is a link to the northwestward migrating Walker Lane belt by inferring fault-slip changes that may track in age with its propagation northward. We further speculate that the global climate shift ca. 4–2 Ma to a more variable climate state could have helped facilitate channel incision (Whipple et al., 1999; Zhang et al., 2001). However, the geomorphic signal associated with such a climate shift is difficult to deconvolve and may have actually resulted in the opposite consequence of reduced fluvial and hillslope gradients, thus providing more support for a tectonic mechanism.

CONCLUSIONS

Basin and Range footwall topography in northwestern Nevada appears to be in a transient state. Our observations show that base level dropped substantially (~220 m) since the Pliocene, resulting in a wave of incision that formed intramontane fluvial knickpoints that segment steep, fault-proximal channel reaches and hillslopes from lower-gradient upstream regions. As the knickpoints migrated upstream, a volume of ~0.5 km^3 of rock was removed from the footwall catchments since ca. 5–0.1 Ma. These results are supported by a knickpoint migration model combined with existing erosion rate estimates that suggest the knickpoints traveled at rates of 0.5–2 mm/yr. We suggest that these geomorphic phenomena result from enhanced fault slip on several normal-fault systems, perhaps in response to the evolving western North American tectonic boundary and/or evolving fault-system geometries. The collective geomorphic evidence is consistent with a phase of faulting previously undocumented using solely thermochronology. We suggest that catchment- to channel-scale geomorphic approaches such as those used here have the potential to improve constraints on fault-motion histories throughout the Basin and Range, bridging the gap between fault initiation and trench-based millennial time scales, and perhaps identifying more new phases of fault motion and topographic growth. Finally, our results bring up new questions and hypotheses about Pliocene–Quaternary landscape change in the Great Basin that we hope inspire future research.

ACKNOWLEDGMENTS

M. Ellis thanks the University of North Carolina Department of Geological Sciences Martin Fund, Geological Society of America, and Sigma Xi for financial support. Julia Ellis and Jim Mize provided valuable help in the field. We thank Andy Cyr, Karl Wegmann, and Sean Gallen for their advice and input and reviewers Nancye Dawers, Scott Miller, Michael Oskin, and an anonymous reviewer for their very constructive reviews.

REFERENCES CITED

Adams, K.D., and Wesnousky, S.G., 1999, The Lake Lahontan highstand: Age, surficial characteristics, soil development, and regional shoreline correlation: Geomorphology, v. 30, no. 4, p. 357–392, doi:10.1016/S0169-555X(99)00031-8.

Allen, G.H., Barnes, J.B., Pavelsky, T.M., and Kirby, E., 2013, Lithologic and tectonic controls on bedrock channel form at the northwest Himalayan front: Journal of Geophysical Research–Earth Surface, v. 118, no. 3, p. 1806–1825, doi:10.1002/jgrf.20113.

Attal, M., Tucker, G.E., Whittaker, A.C., Cowie, P.A., and Roberts, G.P., 2008, Modeling fluvial incision and transient landscape evolution: Influence of dynamic channel adjustment: Journal of Geophysical Research–Earth Surface, v. 113, no. F3, F03013, doi:10.1029/2007JF000893.

Atwater, T., 1970, Implications of plate tectonics for the Cenozoic tectonic evolution of western North America: Geological Society of America Bulletin, v. 81, no. 12, p. 3513–3535, doi:10.1130/0016-7606(1970)81[3513:IOPTFT]2.0.CO;2.

Atwater, T., and Stock, J., 1998, Pacific–North America plate tectonics of the Neogene southwestern United States: An update: International Geology Review, v. 40, no. 5, p. 375–402, doi:10.1080/00206819809465216.

Berlin, M.M., and Anderson, R.S., 2007, Modeling of knickpoint retreat on the Roan Plateau, western Colorado: Journal of Geophysical Research–Earth Surface, v. 112, no. F3, p. F03S06, doi:10.1029/2006JF000553.

Binnie, S.A., Phillips, W.M., Summerfield, M.A., and Fifield, L.K., 2007, Tectonic uplift, threshold hillslopes, and denudation rates in a developing mountain range: Geology, v. 35, no. 8, p. 743–746, doi:10.1130/G23641A.1.

Bishop, P., Hoey, T.B., Jansen, J.D., and Artza, I., 2005, Knickpoint recession rate and catchment area: The case of uplifted rivers in eastern Scotland: Earth Surface Processes and Landforms, v. 30, no. 6, p. 767–778, doi:10.1002/esp.1191.

Bonnet, S., and Crave, A., 2003, Landscape response to climate change: Insights from experimental modeling and implications for tectonic versus climatic uplift of topography: Geology, v. 31, no. 2, p. 123–126, doi:10.1130/0091-7613(2003)031<0123:LRTCCI>2.0.CO;2.

Brueseke, M., Hart, W., and Heizler, M., 2008, Diverse mid-Miocene silicic volcanism associated with the Yellowstone–Newberry thermal anomaly: Bulletin of Volcanology, v. 70, no. 3, p. 343–360, doi:10.1007/s00445-007-0142-5.

Burbank, D.W., Leland, J., Fielding, E., Anderson, R.S., Brozovic, N., Reid, M.R., and Duncan, C., 1996, Bedrock incision, rock uplift and threshold hillslopes in the northwestern Himalayas: Nature, v. 379, no. 6565, p. 505–510, doi:10.1038/379505a0.

Cartwright, J.A., Trudgill, B.D., and Mansfield, C.S., 1995, Fault growth by segment linkage—An explanation for scatter in maximum displacement and trace length data from the Canyonlands grabens of SE Utah: Journal of Structural Geology, v. 17, no. 9, p. 1319–1326, doi:10.1016/0191-8141(95)00033-A.

Cashman, P.H., and Fontaine, S.A., 2000, Strain partitioning in the northern Walker Lane, western Nevada and northeastern California: Tectonophysics, v. 326, no. 1–2, p. 111–130, doi:10.1016/S0040-1951(00)00149-9.

Cassel, E.J., Graham, S.A., Chamberlain, C.P., and Henry, C.D., 2012, Early Cenozoic topography, morphology, and tectonics of the northern Sierra Nevada and western Basin and Range: Geosphere, v. 8, no. 2, p. 229–249, doi:10.1130/GES00671.1.

Castor, S.B., and Henry, C.D., 2000, Geology, geochemistry, and origin of volcanic rock–hosted uranium deposits in northwestern Nevada and southeastern Oregon, USA: Ore Geology Reviews, v. 16, no. 1–2, p. 1–40, doi:10.1016/S0169-1368(99)00021-9.

Chamberlain, C.P., Mix, H.T., Mulch, A., Hren, M.T., Kent-Corson, M.L., Davis, S.J., Horton, T.W., and Graham, S.A., 2012, The Cenozoic climatic and topographic evolution of the western North American Cordillera: American Journal of Science, v. 312, no. 2, p. 213–262, doi:10.2475/02.2012.05.

Clark, M.K., Maheo, G., Saleeby, J., and Farley, K.A., 2005, The non-equilibrium landscape of the southern Sierra Nevada, California: GSA Today, v. 15, no. 9, p. 4, doi:10:1130/1052–5173(2005)015<4:TNELOT>2.0.CO;2.

Clarke, B.A., and Burbank, D.W., 2011, Quantifying bedrock-fracture patterns within the shallow subsurface: Implications for rock mass strength, bedrock landslides, and erodibility: Journal of Geophysical Research–Earth Surface, v. 116, F04009, doi:10.1029/2011JF001987.

Colgan, J.P., 2013, Reappraisal of the relationship between the northern Nevada rift and Miocene extension in the northern Basin and Range Province: Geology, v. 41, no. 2, p. 211–214, doi:10.1130/G33512.1.

Colgan, J.P., and Henry, C.D., 2009, Rapid middle Miocene collapse of the Mesozoic orogenic plateau in north-central Nevada: International Geology Review, v. 51, no. 9–11, p. 920–961, doi:10.1080/00206810903056731.

Colgan, J.P., Dumitru, T.A., and Miller, E.L., 2004, Diachroneity of Basin and Range extension and Yellowstone hotspot volcanism in northwestern Nevada: Geology, v. 32, no. 2, p. 121–124, doi:10.1130/G20037.1.

Colgan, J.P., Dumitru, T.A., McWilliams, M., and Miller, E.L., 2006a, Timing of Cenozoic volcanism and Basin and Range extension in northwestern Nevada: New constraints from the northern Pine Forest Range: Geological Society of America Bulletin, v. 118, no. 1–2, p. 126–139, doi:10.1130/B25681.1.

Colgan, J.P., Dumitru, T.A., Reiners, P.W., Wooden, J.L., and Miller, E.L., 2006b, Cenozoic tectonic evolution of the Basin and Range Province in northwestern Nevada: American Journal of Science, v. 306, no. 8, p. 616–654, doi:10.2475/08.2006.02.

Colgan, J.P., Shuster, D.L., and Reiners, P.W., 2008, Two-phase Neogene extension in the northwestern Basin and Range recorded in a single thermochronology sample: Geology, v. 36, no. 8, p. 631–634, doi:10.1130/G24897A.1.

Cowie, P.A., 1998, A healing–reloading feedback control on the growth rate of seismogenic faults: Journal of Structural Geology, v. 20, no. 8, p. 1075–1087, doi:10.1016/S0191-8141(98)00034-0.

Cowie, P.A., and Roberts, G.P., 2001, Constraining slip rates and spacings for active normal faults: Journal of Structural Geology, v. 23, no. 12, p. 1901–1915, doi:10.1016/S0191-8141(01)00036-0.

Crafford, A.E.J., 2010, Geological Terrane Map of Nevada: Nevada Bureau of Mines and Geology, Open-File Report 10-4; Reno, Nevada; plate 1, scale 1:500,000.

Crosby, B.T., and Whipple, K.X., 2006, Knickpoint initiation and distribution within fluvial networks: 236 waterfalls in the Waipaoa River, North Island, New Zealand: Geomorphology, v. 82, no. 1–2, p. 16–38, doi:10.1016/j.geomorph.2005.08.023.

Cyr, A.J., Granger, D.E., Olivetti, V., and Molin, P., 2010, Quantifying rock uplift rates using channel steepness and cosmogenic nuclide–determined erosion rates: Examples from northern and southern Italy: Lithosphere, v. 2, no. 3, p. 188–198, doi:10.1130/L96.1.

Daly, C., Halbleib, M., Smith, J.I., Gibson, W.P., Doggett, M.K., Taylor, G.H., Curtis, J., and Pasteris, P.A., 2008, Physiographically-sensitive mapping of temperature and precipitation across the conterminous United States: International Journal of Climatology, v. 28, p. 2031–2064, doi:10.1002/joc.1688.

Dawers, N.H., and Anders, M.H., 1995, Displacement-length scaling and fault linkage: Journal of Structural Geology, v. 17, no. 5, p. 607–614, doi:10.1016/0191-8141(94)00091-D.

Dawers, N.H., Anders, M.H., and Scholz, C.H., 1993, Growth of normal faults: Displacement-length scaling: Geology, v. 21, no. 12, p. 1107–1110, doi:10.1130/0091-7613(1993)021<1107:GONFDL>2.3.CO;2.

DeCelles, P.G., 2004, Late Jurassic to Eocene evolution of the Cordilleran thrust belt and foreland basin system, western U.S.: American Journal of Science, v. 304, no. 2, p. 105–168, doi:10.2475/ajs.304.2.105.

Densmore, A.L., Dawers, N.H., Gupta, S., Guidon, R., and Goldin, T., 2004, Footwall topographic development during continental extension: Journal of Geophysical Research, v. 109, F03001, doi:10.1029/2003JF000115.

Densmore, A.L., Dawers, N.H., Gupta, S., and Guidon, R., 2005, What sets topographic relief in extensional footwalls?: Geology, v. 33, no. 6, p. 453–456, doi:10.1130/G21440.1.

Densmore, A.L., Hetzel, R., Ivy-Ochs, S., Krugh, W.C., Dawers, N., and Kubik, P., 2009, Spatial variations in catchment-averaged denudation rates from normal fault footwalls: Geology, v. 37, no. 12, p. 1139–1142, doi:10.1130/G30164A.1.

Dumitru, T.A., 2000, Fission-track geochronology, *in* Noller, J.S., Sowers, J.M., and Lettis, W.R., eds., Quaternary Geochronology: Methods and Applications: American Geophysical Union Reference Shelf Volume 4, p. 131–155.

Duvall, A., Kirby, E., and Burbank, D., 2004, Tectonic and lithologic controls on bedrock channel profiles and processes in coastal California: Journal of Geophysical Research, v. 109, F03002, doi:10.1029/2003JF000086.

Ehlers, J., and Gibbard, P.L., 2007, The extent and chronology of Cenozoic global glaciation: Quaternary International, v. 164–165, p. 6–20, doi:10.1016/j.quaint.2006.10.008.

Ehlers, T.A., and Farley, K.A., 2003, Apatite (U-Th)/He thermochronometry; methods and applications to problems in tectonic and surface processes: Earth and Planetary Science Letters, v. 206, no. 1–2, p. 1–14, doi:10.1016/S0012-821X(02)01069-5.

Ehlers, T.A., Armstrong, P.A., and Chapman, D.S., 2001, Normal fault thermal regimes and the interpretation of low-temperature thermochronometers: Physics of the Earth and Planetary Interiors, v. 126, p. 179–194.

Ellis, M.A., Densmore, A.L., and Anderson, R.S., 1999, Development of mountainous topography in the Basin and Ranges, USA: Basin Research, v. 11, no. 1, p. 21–41, doi:10.1046/j.1365-2117.1999.00087.x.

England, P., and Molnar, P., 1990, Surface uplift, uplift of rocks, and exhumation of rocks: Geology, v. 18, no. 12, p. 1173–1177, doi:10.1130/0091-7613(1990)018<1173:SUUORA>2.3.CO;2.

Farley, K.A., 2002, (U-Th)/He dating: Techniques, calibrations, and applications, *in* Portcelli, D., Ballentine, C.J., and Wieler, R., eds., Noble Gases in Geochemistry and Cosmochemistry, Volume 47: Washington, D.C., Mineralogical Society of America, p. 819–843.

Faulds, J.E., Henry, C.D., and Hinz, N.H., 2005, Kinematics of the northern Walker Lane: An incipient transform fault along the Pacific–North American plate boundary: Geology, v. 33, no. 6, p. 505–508, doi:10.1130/G21274.1.

Flint, J.J., 1974, Stream gradient as a function of order, magnitude, and discharge: Water Resources Research, v. 10, no. 5, p. 969–973, doi:10.1029/WR010i005p00969.

Frankel, K.L., Dolan, J.F., Owen, L.A., Ganev, P., and Finkel, R.C., 2011, Spatial and temporal constancy of seismic strain release along an evolving segment of the Pacific–North America plate boundary: Earth and Planetary Science Letters, v. 304, no. 3–4, p. 565–576, doi:10.1016/j.epsl.2011.02.034.

Gallen, S.F., Wegmann, K.W., and Bohnenstiehl, D.R., 2013, Miocene rejuvenation of topographic relief in the southern Appalachians: GSA Today, v. 23, no. 2, p. 4–10, doi:10.1130/GSATG163A.1.

Gesch, D.B., 2007, The National Elevation Dataset, *in* Maune, D., ed., Digital Elevation Model Technologies and Applications: The DEM Users' Manual: Bethesda, Maryland, American Society for Photogrammetry and Remote Sensing, p. 99–118.

Gesch, D.B., Oimoen, M., Greenlee, S., Nelson, C., Steuck, M., and Tyler, D., 2002, The National Elevation Dataset: Photogrammetric Engineering and Remote Sensing, v. 68, no. 1, p. 5–11.

Goren, L., Fox, M., and Willett, S.D., 2014, Tectonics from fluvial topography using formal linear inversion: Theory and applications to the Inyo Mountains, California: Journal of Geophysical Research–Earth Surface, v. 119, no. 8, p. 1651–1681, doi:10.1002/2014jf003079.

Gorynski, K.E., Stockli, D.F., and Walker, J.D., 2013, Thermochronometrically constrained anatomy and evolution of a Miocene extensional accommodation zone and tilt domain boundary: The southern Wassuk Range, Nevada: Tectonics, v. 32, no. 3, p. 516–539, doi:10.1002/tect.20044.

Goudie, A.S., 2006, The Schmidt hammer in geomorphological research: Progress in Physical Geography, v. 30, no. 6, p. 703–718, doi:10.1177/0309133306071954.

Green, P., Duddy, I., Laslett, G., Hegarty, K., Gleadow, A., and Lovering, J., 1989, Thermal annealing of fission tracks in apatite: 4. Quantitative modelling techniques and extension to geological timescales: Chemical Geology–Isotope Geoscience Section, v. 79, no. 2, p. 155–182, doi:10.1016/0168-9622(89)90018-3.

Gupta, A., and Scholz, C.H., 2000, A model of normal fault interaction based on observations and theory: Journal of Structural Geology, v. 22, no. 7, p. 865–879, doi:10.1016/S0191-8141(00)00011-0.

Hack, J.T., 1973, Stream-profile analysis and stream-gradient index: Journal of Research of the U.S. Geological Survey, v. 1, p. 421–429.

Harbor, D.J., 1997, Landscape evolution at the margin of the Basin and Range: Geology, v. 25, no. 12, p. 1111–1114, doi:10.1130/0091-7613(1997)025<1111:LEATMO>2.3.CO;2.

Harkins, N., Kirby, E., Heimsath, A., Robinson, R., and Reiser, U., 2007, Transient fluvial incision in the headwaters of the Yellow River, northeastern Tibet, China: Journal of Geophysical Research–Earth Surface, v. 112, no. F3, F03S04, doi:10.1029/2006JF000570.

Harrison, C.G.A., 2000, What factors control mechanical erosion rates?: International Journal of Earth Sciences, v. 88, no. 4, p. 752–763, doi:10.1007/s005310050303.

Haviv, I., Enzel, Y., Whipple, K.X., Zilberman, E., Matmon, A., Stone, J., and Fifield, K.L., 2010, Evolution of vertical knickpoints (waterfalls) with resistant caprock: Insights from numerical modeling: Journal of Geophysical Research–Earth Surface, v. 115, no. F3, F03028, doi:10.1029/2008JF001187.

Hayakawa, Y., and Matsukura, Y., 2003, Recession rates of waterfalls in Boso Peninsula, Japan, and a predictive equation: Earth Surface Processes and Landforms, v. 28, no. 6, p. 675–684, doi:10.1002/esp.519.

Hemphill-Haley, M.A., Sawyer, T.L., Knuepfer, P.L.K., Forman, S.L., and Wong, I.G., 2000, Timing of faulting events from thermoluminescence dating of scarp-related deposits, Lemhi fault, southeastern Idaho, *in* Noller, J.S., Sowers, J.M., and Lettis, W.R., eds., Quaternary Geochronology: Methods and Applications: American Geophysical Union Reference Shelf Volume 4, p. 541–548.

Henry, C.D., and Perkins, M.E., 2001, Sierra Nevada–Basin and Range transition near Reno, Nevada: Two-stage development at 12 and 3 Ma: Geology, v. 29, no. 8, p. 719–722, doi:10.1130/0091-7613(2001)029<0719:snbart>2.0.co;2.

Henry, C.D., Faulds, J.E., and dePolo, C.M., 2007, Geometry and timing of strike-slip and normal faults in the northern Walker Lane, northwestern Nevada and northeastern California: Strain partitioning or sequential extensional and strike-slip deformation?, *in* Till, A.B., Roeske, S.M., Sample, J.C., and Foster, D.A., eds., Exhumation Associated with Continental Strike-Slip Fault Systems: Geological Society of America Special Paper 434, p. 59–79, doi:10.1130/2007.2434(04).

Horton, T.W., Sjostrom, D.J., Abruzzese, M.J., Poage, M.A., Waldbauer, J.R., Hren, M., Wooden, J., and Chamberlain, C.P., 2004, Spatial and temporal variation of Cenozoic surface elevation in the Great Basin and Sierra Nevada: American Journal of Science, v. 304, no. 10, p. 862–888, doi:10.2475/ajs.304.10.862.

Kirby, E., and Whipple, K.X., 2012, Expression of active tectonics in erosional landscapes: Journal of Structural Geology, v. 44, p. 54–75, doi:10.1016/j.jsg.2012.07.009.

Kirby, E., Regalla, C., Ouimet, W.B., and Bierman, P.R., 2010, Reconstructing temporal variation in fault slip from footwall topography: An example from Saline Valley, California: San Francisco, California, American Geophysical Union, Fall Meeting 2010, abstract EP44A-05.

Korup, O., 2006, Rock-slope failure and the river long profile: Geology, v. 34, no. 1, p. 45–48, doi:10.1130/G21959.1.

Lague, D., Hovius, N., and Davy, P., 2005, Discharge, discharge variability, and the bedrock channel profile: Journal of Geophysical Research–Earth Surface, v. 110, no. F4, F04006, doi:10.1029/2004JF000259.

Lerch, D.W., Miller, E., McWilliams, M., and Colgan, J., 2008, Tectonic and magmatic evolution of the northwestern Basin and Range and its transition to unextended volcanic plateaus: Black Rock Range, Nevada: Geological Society of America Bulletin, v. 120, no. 3–4, p. 300–311, doi:10.1130/B26151.1.

Lifton, Z.M., Newman, A.V., Frankel, K.L., Johnson, C.W., and Dixon, T.H., 2013, Insights into distributed plate rates across the Walker Lane from GPS geodesy: Geophysical Research Letters, v. 40, no. 17, p. 4620–4624, doi:10.1002/grl.50804.

Loget, N., and Van Den Driessche, J., 2009, Wave train model for knickpoint migration: Geomorphology, v. 106, no. 3–4, p. 376–382, doi:10.1016/j.geomorph.2008.10.017.

Matsubara, Y., and Howard, A.D., 2014, Modeling planform evolution of a mud-dominated meandering river: Quinn River, Nevada, USA: Earth Surface Processes and Landforms, v. 39, no. 10, p. 1365–1377, doi:10.1002/esp.3588.

McLeod, A.E., Dawers, N.H., and Underhill, J.R., 2000, The propagation and linkage of normal faults: Insights from the Strathspey–Brent–Statfjord fault array, northern North Sea: Basin Research, v. 12, no. 3–4, p. 263–284, doi:10.1046/j.1365-2117.2000.00124.x.

Miller, E.L., Dumitru, T.A., Brown, R.W., and Gans, P.B., 1999, Rapid Miocene slip on the Snake Range–Deep Creek Range fault system, east-central Nevada: Geological Society of America Bulletin, v. 111, no. 6, p. 886–905, doi:10.1130/0016-7606(1999)111<0886:RMSOTS>2.3.CO;2.

Miller, S.R., Baldwin, S.L., and Fitzgerald, P.G., 2012, Transient fluvial incision and active surface uplift in the Woodlark Rift of eastern Papua New Guinea: Lithosphere, v. 4, no. 2, p. 131–149, doi:10.1130/L135.1.

Molnar, P., and England, P.C., 1990, Late Cenozoic uplift of mountain ranges and global climate change; chicken or egg?: Nature, v. 346, no. 6279, p. 29–34, doi:10.1038/346029a0.

Montgomery, D.R., and Brandon, M.T., 2002, Topographic controls on erosion rates in tectonically active mountain ranges: Earth and Planetary Science Letters, v. 201, no. 3–4, p. 481–489, doi:10.1016/S0012-821X(02)00725-2.

Montgomery, D.R., and Gran, K.B., 2001, Downstream variations in the width of bedrock channels: Water Resources Research, v. 37, no. 6, p. 1841–1846, doi:10.1029/2000WR900393.

Morrison, R.B., 1991, Quaternary stratigraphic, hydrologic, and climatic history of the Great Basin, with emphasis on Lakes Lahontan, Bonneville, and Tecopa, *in* Morrison, R.B., ed., Quaternary Nonglacial Geology: Conterminous U.S.: Boulder, Colorado, Geological Society of America, The Geology of North America, v. K-2, p. 283–320.

Niemann, J.D., Gasparini, N.M., Tucker, G.E., and Bras, R.L., 2001, A quantitative evaluation of Playfair's law and its use in testing long-term stream erosion models: Earth Surface Processes and Landforms, v. 26, no. 12, p. 1317–1332, doi:10.1002/esp.272.

Noble, D.C., McKee, E.H., Smith, J.G., and Korringa, M.K., 1970, Stratigraphy and Geochronology of Miocene Volcanic Rocks in Northwestern Nevada: U.S. Geological Survey Professional Paper 700D, p. 23–32.

Norton, K.P., von Blanckenburg, F., Schlunegger, F., Schwab, M., and Kubik, P.W., 2008, Cosmogenic nuclide–based investigation of spatial erosion and hillslope channel coupling in the transient foreland of the Swiss Alps: Geomorphology, v. 95, no. 3–4, p. 474–486, doi:10.1016/j.geomorph.2007.07.013.

Ouimet, W.B., Whipple, K.X., and Granger, D.E., 2009, Beyond threshold hillslopes: Channel adjustment to base-level fall in tectonically active mountain ranges: Geology, v. 37, no. 7, p. 579–582, doi:10.1130/G30013A.1.

Personius, S.F., and Mahan, S.A., 2005, Unusually low rates of slip on the Santa Rosa Range fault zone, northern Nevada: Bulletin of the Seismological Society of America, v. 95, no. 1, p. 319–334, doi:10.1785/0120040001.

Poage, M.A., and Chamberlain, C.P., 2002, Stable isotopic evidence for a pre–middle Miocene rain shadow in the western Basin and Range: Implications for the paleotopography of the Sierra Nevada: Tectonics, v. 21, no. 4, p. 16-11–16-10, doi:10.1029/2001tc001303.

Quinn, M.J., Wright, J.E., and Wyld, S.J., 1997, Happy Creek igneous complex and tectonic evolution of the early

Mesozoic arc in the Jackson Mountains, northwest Nevada: Geological Society of America Bulletin, v. 109, no. 4, p. 461–482, doi:10.1130/0016-7606(1997)109<0461:HCICAT>2.3.CO;2.

Reheis, M., 1999a, Extent of Pleistocene Lakes in the Western Great Basin: U.S. Geological Survey Miscellaneous Field Investigations Map MF-2323, scale 1:800,000.

Reheis, M., 1999b, Highest pluvial-lake shorelines and Pleistocene climate of the western Great Basin: Quaternary Research, v. 52, no. 2, p. 196–205, doi:10.1006/qres.1999.2064.

Reiners, P.W., and Ehlers, T.A., eds., 2005, Low-temperature thermochronology: Techniques, Interpretations, and Applications: Mineralogical Society of America, Reviews in Mineralogy and Geochemistry Volume 58, 622 p.

Ring, U., Brandon, M.T., Willett, S.D., and Lister, G.S., 1999, Exhumation processes, *in* Ring, U., Brandon, M.T., Lister, G.S., and Willett, S.D., eds., Exhumation Processes; Normal Faulting, Ductile Flow and Erosion: Geological Society of London Special Publication 154, p. 1–27.

Rosenbloom, N.A., and Anderson, R.S., 1994, Hillslope and channel evolution in a marine terraced landscape, Santa Cruz, California: Journal of Geophysical Research, v. 99, no. B7, p. 14,013–14,029, doi:10.1029/94JB00048.

Schmidt, K.M., and Montgomery, D.R., 1995, Limits to relief: Science, v. 270, no. 5236, p. 617–620, doi:10.1126/science.270.5236.617.

Selby, M.J., 1993, Hillslope Materials and Processes (2nd ed.): Oxford, UK, Oxford University Press, 451 p.

Shackleton, N.J., Backman, J., Zimmerman, H., Kent, D.V., Hall, M.A., Roberts, D.G., Schnitker, D., Baldauf, J.G., Desprairies, A., and Homrighausen, R., 1984, Oxygen isotope calibration of the onset of ice-rafting and history of glaciation in the North Atlantic region: Nature, v. 307, no. 5952, p. 620–623, doi:10.1038/307620a0.

Sklar, L.S., and Dietrich, W.E., 2001, Sediment and rock strength controls on river incision into bedrock: Geology, v. 29, no. 12, p. 1087–1090, doi:10.1130/0091-7613(2001)029<1087:SARSCO>2.0.CO;2.

Snow, J., and Wernicke, B., 2000, Cenozoic tectonism in the central Basin and Range; magnitude, rate, and distribution of upper crustal strain: American Journal of Science, v. 300, no. 9, p. 659–719, doi:10.2475/ajs.300.9.659.

Stark, C.P., Barbour, J.R., Hayakawa, Y.S., Hattanji, T., Hovius, N., Chen, H., Lin, C.-W., Horng, M.-J., Xu, K.-Q., and Fukahata, Y., 2010, The climatic signature of incised river meanders: Science, v. 327, no. 5972, p. 1497–1501, doi:10.1126/science.1184406.

Stewart, J.H., 1971, Basin and Range structure: A system of horsts and grabens produced by deep-seated extension: Geological Society of America Bulletin, v. 82, p. 1019–1044, doi:10.1130/0016-7606(1971)82[1019:BARSAS]2.0.CO;2.

Stewart, M., and Crowell, J.C., 1992, Strike-slip tectonics in the Cordilleran region, western United States, *in* Burchfiel, B.C., Lipman, P.W., and Zoback, M.L., eds., The Cordilleran Orogen: Conterminous U.S.: Boulder, Colorado, Geological Society of America, The Geology of North America, v. G-3, p. 609–628.

Stock, G.M., Anderson, R.S., and Finkel, R.C., 2005, Rates of erosion and topographic evolution of the Sierra Nevada, California, inferred from cosmogenic ^{26}Al and ^{10}Be concentrations: Earth Surface Processes and Landforms, v. 30, no. 8, p. 985–1006, doi:10.1002/esp.1258.

Stockli, D.F., 2005, Application of low-temperature thermochronometry to extensional tectonic settings, *in* Reiners, P.W., and Ehlers, T.A., eds., Low-Temperature Thermochronology: Techniques, Interpretations, & Applications: Mineralogical Society of America, Reviews in Mineralogy and Geochemistry Volume 58, p. 411–448.

Stockli, D.F., Surpless, B.E., Dumitru, T.A., and Farley, K., 2002, Thermochronological constraints on the timing and magnitude of Miocene and Pliocene extension in the central Wassuk Range, western Nevada: Tectonics, v. 21, no. 4, p. 10-1–10-19, doi:10.1029/2001TC001295.

Stockli, D.F., Dumitru, T.A., McWilliams, M.O., and Farley, K.A., 2003, Cenozoic tectonic evolution of the White Mountains, California and Nevada: Geological Society of America Bulletin, v. 115, no. 7, p. 788–816, doi:10.1130/0016-7606(2003)115<0788:CTEOTW>2.0.CO;2.

Tucker, G.E., and Whipple, K.X., 2002, Topographic outcomes predicted by stream erosion models: Sensitivity analysis and intermodel comparison: Journal of Geophysical Research, v. 107, no. B9, p. 2179, doi:10.1029/2001JB000162.

Wakabayashi, J., and Sawyer, T.L., 2001, Stream incision, tectonics, uplift, and evolution of topography of the Sierra Nevada, California: The Journal of Geology, v. 109, no. 5, p. 539–562, doi:10.1086/321962.

Wallace, R.E., 1987, Grouping and migration of surface faulting and variations in slip rates on faults in the Great Basin Province: Bulletin of the Seismological Society of America, v. 77, p. 868–876.

Walsh, L.S., Martin, A.J., Ojha, T.P., and Fedenczuk, T., 2012, Correlations of fluvial knickzones with landslide dams, lithologic contacts, and faults in the southwestern Annapurna Range, central Nepalese Himalaya: Journal of Geophysical Research–Earth Surface, v. 117, no. F1, F01012, doi:10.1029/2011JF001984.

Wernicke, B., 1992, Cenozoic extensional tectonics of the U.S. Cordillera, *in* Burchfiel, B.C., Lipman, P.W., and Zoback, M.L., eds., The Cordilleran Region: Boulder, Colorado, Geological Society of America, The Geology of North America, v. G-3, p. 553–581

Whipple, K.X., 2001, Fluvial landscape response time: How plausible is steady-state denudation?: American Journal of Science, v. 301, no. 4–5, p. 313–325, doi:10.2475/ajs.301.4-5.313.

Whipple, K.X., 2004, Bedrock rivers and the geomorphology of active orogens: Annual Review of Earth and Planetary Sciences, v. 32, p. 151–185, doi:10.1146/annurev.earth.32.101802.120356.

Whipple, K.X., and Trayler, C.R., 1996, Tectonic control of fan size; the importance of spatially variable subsidence rates: Basin Research, v. 8, no. 3, p. 351–366, doi:10.1046/j.1365-2117.1996.00129.x.

Whipple, K.X., and Tucker, G., 1999, Dynamics of the stream-power river incision model; implications for height limits of mountain ranges, landscape response timescales, and research needs: Journal of Geophysical Research, v. 104, no. B8, p. 17,661–17,674, doi:10.1029/1999JB900120.

Whipple, K.X., Kirby, E., and Brocklehurst, S.H., 1999, Geomorphic limits to climate-induced increases in topographic relief: Nature, v. 401, no. 6748, p. 39–43, doi:10.1038/43375.

Whittaker, A.C., 2012, How do landscapes record tectonics and climate?: Lithosphere, v. 4, no. 2, p. 160–164, doi:10.1130/RF.L003.1.

Whittaker, A.C., Attal, M., Cowie, P.A., Tucker, G.E., and Roberts, G., 2008, Decoding temporal and spatial patterns of fault uplift using transient river long profiles: Geomorphology, v. 100, no. 3–4, p. 506–526, doi:10.1016/j.geomorph.2008.01.018.

Willett, S.D., McCoy, S.W., Perron, J.T., Goren, L., and Chen, C.-Y., 2014, Dynamic reorganization of river basins: Science, v. 343, no. 6175, doi:10.1126/science.1248765.

Wobus, C.W., Whipple, K.X., Kirby, E., Snyder, N., Johnson, J., Spyropolou, K., Crosby, B., and Sheehan, D., 2006a, Tectonics from topography; procedures, promise, and pitfalls, *in* Willett, S.D., Hovius, N., Brandon, M.T., and Fisher, D.M., eds., Tectonics, Climate and Landscape Evolution: Geological Society of America Special Paper 398, p. 55–74.

Wobus, C.W., Crosby, B.T., and Whipple, K.X., 2006b, Hanging valleys in fluvial systems: Controls on occurrence and implications for landscape evolution: Journal of Geophysical Research–Earth Surface, v. 111, no. F2, F02017, doi:10.1029/2005JF000406.

Wolf, R., Farley, K., and Kass, D., 1998, Modeling of the temperature sensitivity of the apatite (U-Th)/He thermochronometer: Chemical Geology, v. 148, no. 1–2, p. 105–114, doi:10.1016/S0009-2541(98)00024-2.

Wyld, S.J., 1996, Early Jurassic deformation in the Pine Forest Range, northwest Nevada, and implications for Cordilleran tectonics: Tectonics, v. 15, no. 3, p. 566–583, doi:10.1029/95TC03693.

Zhang, P., Molnar, P., and Downs, W.R., 2001, Increased sedimentation rates and grain sizes 2–4 Myr ago due to the influence of climate change on erosion rates: Nature, v. 410, no. 6831, p. 891–897, doi:10.1038/35073504.

MANUSCRIPT RECEIVED 11 JUNE 2014
REVISED MANUSCRIPT RECEIVED 3 OCTOBER 2014
MANUSCRIPT ACCEPTED 7 NOVEMBER 2014

Printed in the USA